Available online at www.sciencedirect.com
ScienceDirect
International Journal of Heat and Mass Transfer 51 (2008) 2237–2259
International Journal of HEAT and MASS TRANSFER
www.elsevier.com/locate/ijhmt

Non-Fourier analysis of skin biothermomechanics

F. Xu [a], K.A. Seffen [a], T.J. Lu [b,*]

[a] Engineering Department, Cambridge University, Cambridge CB2 1PZ, UK
[b] MOE Key Laboratory of Strength and Vibration, School of Aerospace, Xi'an Jiaotong University, Xi'an 710049, PR China

Received 30 January 2007; received in revised form 26 October 2007
Available online 26 December 2007

Abstract

Biothermomechanics of skin is highly interdisciplinary, involving bioheat transfer, burn damage, biomechanics and physiology. Comprehension of the phenomena of heat transfer and related thermomechanics in skin tissue is of great importance and can contribute to a variety of medical applications. Due to the "lengthy" thermal relaxation time in biological tissue, non-Fourier thermal behaviour has been experimentally observed, attracting increasingly more attention to this phenomenon. The aim of this study is to review previous researches on the non-Fourier heat transfer process and to develop a computational approach to examine this non-Fourier process and its influence on the mechanical response in skin tissue. The dual-phase-lag (DPL) model is first used to model bioheat transfer across the tissue. Together with the thermal wave model, the non-Fourier thermomechanical behaviour of the tissue is analyzed under various surface heating boundary conditions. For single-layer tissue model, exact solutions for temperature, thermal stress and thermal damage fields are derived; for multi-layer structural models, numerical solutions are obtained with the finite difference method. Large discrepancies are found to exist amongst the predictions of Pennes model, thermal wave model and dual-phase-lag model, while different DPL bioheat transfer models give similar predictions.

Keywords: Skin tissue; Non-Fourier analysis; Bioheat transfer; Temperature; Thermal stress; Thermal pain; Numerical method

1. Introduction

Epidermis, dermis, and subcutaneous tissue are the main compositions of skin (see Fig. 1a). In addition to sensing, thermoregulation and host defense, the most important role of skin is thermoregulation: skin functions as a generator, absorber, transmitter, radiator, conductor and vaporizer of heat. Thermoregulation makes the skin an important barrier for the human body to various outside conditions. However, in an extreme environment, people may feel uncomfortable, or even pain, when there is extreme heat or cold. Obviously, the skin fails to protect the body when the temperature moves out of the normal physiological range. On the other hand, in medicine, various thermal based therapies are widely used to cure disease/injury involving skin tissue, where thermal injury is induced precisely within the diseased skin tissue but without affecting the surrounding healthy tissue. Thus, extreme thermal behaviour can offer benefits, if controllable, but it requires the following questions to be answered in some way: why do human beings feel uncomfortable/pain, what is happening to the human body, and how to protect the human body in an extreme thermal environment? A detailed understanding of the bio-thermo-mechanical behaviour of skin tissue is therefore of great practical importance.

Thermal behaviour, or, heat transfer, in skin is mainly a heat conduction process coupled to complicated physiological processes, including blood circulation, sweating, metabolic heat generation, and, sometimes, heat dissipation via hair or fur above the skin surface. In many situations, heat conduction has been treated according to the classic Fourier's law, which assumes that any thermal disturbance on a body is instantaneously felt throughout the body or,

* Corresponding author. Tel.: +86 29 82665600; fax: +86 29 83234781.
E-mail address: tjlu@mail.xjtu.edu.cn (T.J. Lu).

0017-9310/$ - see front matter © 2007 Elsevier Ltd. All rights reserved.
doi:10.1016/j.ijheatmasstransfer.2007.10.024

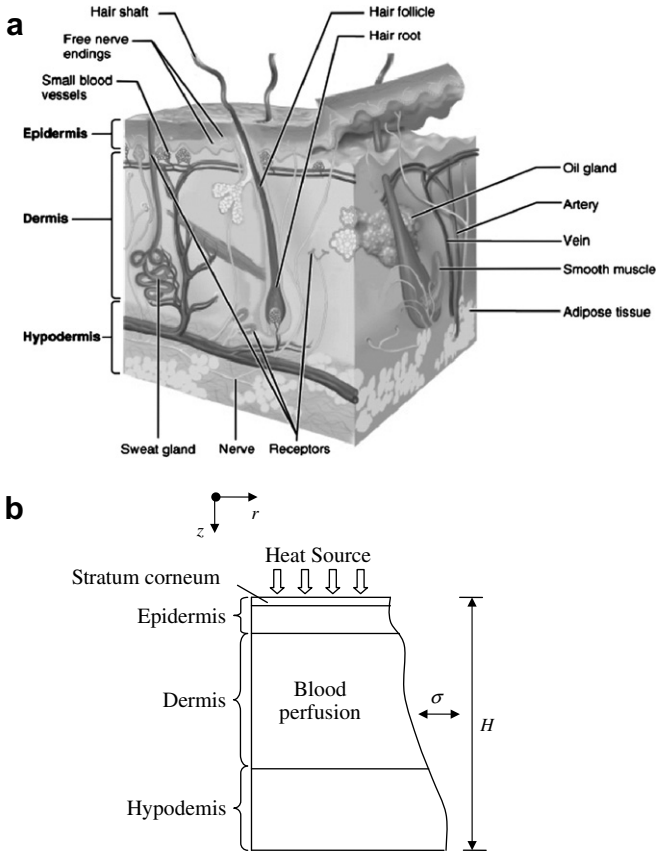

Fig. 1. (a) Skin structure [92] and (b) corresponding idealized skin model.

equivalently, the propagation speed of thermal disturbance is infinite. Although this assumption is reasonable in the majority of practical applications, it fails in particular thermal conditions or heat conduction media, where the heat conduction behaviour shows a non-Fourier feature such as thermal wave phenomenon, or hyperbolic heat conduction as defined mathematically.

Non-Fourier heat conduction behaviour has been experimentally observed in engineering materials or heat conduction media operating at low temperatures, such as liquid Helium II [1] and Al_2O_3 crystal [2], etc. Later, following developments in laser technology, non-Fourier thermal behaviour was observed in short-pulse laser processing of thin-film engineering structures [3,4]. A similar phenomenon has also been experimentally observed in materials with non-homogeneous inner structure [5], such as H acid, $NaHCO_3$, sand, glass ballontini, ion exchange, and sand with an irregular grain structure, which are similar in heterogeneity to biological tissues.

1.1. Non-Fourier heat conduction in non-homogeneous materials

Although non-Fourier heat conduction in materials having a non-homogeneous inner structure has been reported by various researchers, this claim was initially rebutted by Graßmann and Peters [6] and Herwig and Beckers [7,8], for they observed no evidence of hyperbolic conduction in skin tissue. Different investigators however have reported flaws in their experimental philosophy [9], where one limitation was found to be the determination of thermal diffusivity and relaxation time. Accordingly, Roetzel et al. [9] carried out an experiment to simultaneously determine these parameters from a single experiment and their results confirmed a hyperbolic behaviour of thermal propagation, but smaller in extent compared to that reported in the literature.

The non-homogeneous inner structure of biological tissue suggests the existence of non-Fourier heat conduction behaviour, as temperature oscillation (an unusual oscillation of tissue temperature with heating) and wave-like behaviour are commonly observed. Temperature oscillation in living tissue was first observed by Richardson et al. [10] and later by Roemer et al. [11], who subjected canine thigh muscle to an abrupt application of microwave heating at different power levels. Subsequently, Mitra et al. [12] carried out four different experiments with processed meat for different boundary conditions and also observed the wave-like behaviour (temperature jumps which can be regarded as the wave front): (1) tissue temperature rose monotonically with time to an elevated steady state value at low power levels; (2) temperature rose above a 'critical temperature' before an abrupt increase in blood perfusion was activated to reduce the temperature to a new steady state value; (3) temperature responded as damped or self-sustained large oscillations (jumps); (4) temperature increased continuously at a rapid rate at high power levels. On the other hand, Davydov et al. [13] experimentally observed that heat transfer in a muscle tissue under local strong heating exhibits substantial anisotropy, which cannot be explained by the standard Fourier-theory based heat diffusion model. Banerjee et al. [4] measured the thermal response of meat under laser irradiation, and found that the non-Fourier hyperbolic heat conduction equation is a better approximation than the classical parabolic Fourier heat conduction formulation.

As with engineering materials, there are different viewpoints on the non-Fourier behaviour of biological materials. For example, Tilahun et al. [14] and Herwig and Beckert [8] questioned the experimental results of Mitra et al. [12]; the former tried to reproduce Mitra's experiment [12] with processed meat but did not observe any non-Fourier behaviour. In turn, they cited several issues associated with the Mitra's experiments that might have caused the observed temperature jumps. Herwig and Beckert [8] also found no evidence of non-Fourier heat conduction effects, and they pointed out that the thermal lag effect can be explained by the Fourier heat conduction rather than by the wave behaviour. Unfortunately, it was not possible to reconcile the conflicting measurements of Mitra with Tilahun, and Herwig and Beckert, for the experiments were performed differently and there was no information in either study about the processed meats [15].

Although a wave-like heat transfer behaviour in living tissue is intriguing, no ultimate conclusion can be drawn at present due to the complexity of biological systems [16]. Theoretically, treating the non-homogeneous biological material as a porous medium under the same boundary conditions as in one of Mitra's experiments, Xu and Liu [17] found that the wave-like thermal behaviour in the meat may be caused by the convection of water inside the tissue. This aspect was thought to be induced in the experiments of Mitra et al. [12] by pressing the meat samples together at the start of each experiment and by the subsequent development of temperature gradients across the samples. The temperature jumps were attributed to the arrival of warm water at the measurement locations in the colder samples before the effect of "pure conduction" became noticeable at these locations. However, Xu and Liu [17] did not directly compare their predictions with measurements. Davydov et al. [13] also attributed their observation of anomalous heat transfer behaviour in muscle tissue to the flow of interstitial liquid as a result of non-uniform heating. Despite the resemblance between the findings of Mitra et al. [12] and Xu and Liu [17], to interpret the experiments of Mitra in the context of convection rather than "pure conduction" requires additional study.

Alternatively, the temperature oscillation phenomenon has been attributed to blood perfusion oscillation due to heating [11,17–20]. However, this explanation was subsequently questioned by others [16,21]. Using an artificially simulating construction similar to a bioheat transfer system, Liu et al. [22,23] carried out a series of experiments and found that the temperature oscillations can be well fitted with the thermal wave analysis.

1.2. Importance in thermal therapies

Advances in laser, microwave and similar technologies have led to recent developments of thermal treatments for diseased and injured skin tissue, such as skin cancer and skin burn. The objective is to induce thermal injury precisely within tissue structures located several millimeters below the surface but without affecting the surrounding, healthy tissue. The success of these thermal therapies depends on the precise prediction and control of temperature, damage and stress distributions in the tissue.

From a therapeutic viewpoint, the high-intensity short duration heating scheme can efficiently produce an appropriate and precise dose of heat during thermal therapies. In addition, reducing the overall treatment time is important, especially when the treatment target volume is large. A rapid heating scheme with a good strategy is therefore essential for an effective thermal therapy. However, the possible non-Fourier nature of heat transfer in living tissue may play an important role during rapid heating, such as thermal ablation/thermal surgery, when a high-intensity thermal source such as focused laser, ultrasound or radio-frequency is used. For example, it has been shown that the thermal relaxation of tissue will delay the appearance of peak temperature during thermal treatments, leading to a lower thermal dose level [24]. Furthermore, damage to human tissue from thermal agitation is an exponential function of temperature [25], so even small improvements in the prediction of temperature can strongly influence the prediction of damage. Knowledge of temperature distribution is also essential for the understanding of the corresponding thermomechanical behaviour.

In spite of the widespread use of heating therapies in dermatology, they do not draw upon the detailed understanding of the bio-thermo-mechanical behaviour of tissue, for none exists to date, even though each behavioral facet is well established and understood. A detailed understanding of the coupled biological–mechanical response under thermal agitation can contribute to the design, characterization and optimization of strategies for delivering better treatment. Consequently, in this study different non-Fourier heat conduction models are explored to investigate the relationship between thermal relaxation times and the thermomechanical response in skin tissue. However, this work does not seek to prove one model is better (or not) than others; rather, it attempts to address whether non-Fourier models merit additional study. The paper is organized as follows. In Section 2, different non-Fourier heat transfer models for skin thermal behaviour are developed. The methods for quantifying the resulting thermal damage and thermal stress are presented separately in Sections 3 and 4; the corresponding solutions are presented in Section 5. In Section 6, case studies are examined to compare the predictions from different models.

2. Heat transfer models

2.1. Fourier heat equation

For bioheat transfer, the Pennes equation [26] is well-known. The conduction term in this equation is based on the classical Fourier's law, postulated in the publication of Fourier's studies concerning heat conduction:

$$q(\vec{r},t) = -k\nabla T(\vec{r},t) \tag{1}$$

where q is the heat flux vector representing heat flow per unit time, per unit area of the isothermal surface in the direction of the deceasing temperature; k is the thermal conductivity which is a positive, scalar quantity; ∇T is the temperature gradient; $\vec{r}$ stands for the position vector. The general bioheat transfer equation is given as:

$$\rho c\frac{\partial T}{\partial t} = -\nabla q + \varpi_b\rho_b c_b(T_a - T) + q_{met} + q_{ext} \tag{2}$$

where ρ, c, k are the density, specific heat and thermal conductivity of skin tissue, respectively; ρ_b, c_b are the density and specific heat of blood, ϖ_b is the blood perfusion rate; T_a and T are the temperatures of arterial blood and skin tissue respectively; q_{met} is the metabolic heat generation in the skin tissue and q_{ext} is the heat source due to external heating.

2.1.1. Pennes bio-heat transfer equation

By combining Eqs. (1) and (2), we can get the Pennes bioheat transfer equation:

$$\rho c\frac{\partial T}{\partial t} = k\nabla^2 T + \varpi_b \rho_b c_b (T_a - T) + q_{met} + q_{ext} \tag{3}$$

2.1.2. Problems with Fourier's law

Although the Fourier assumption has been employed extensively and successfully, some doubts have been cast on its completeness [27]. In the Fourier law, it is assumed that any temperature disturbance or thermal wave will propagate at an infinite speed through the medium. However, this assumption has been shown to be physically unrealizable since, in reality, any equilibrium state in thermodynamic transition needs time to establish [8,28]. Fourier's law has been shown to fail during the short duration of an initial transient, or when the thermal propagation speed of thermal wave is not high [3], as observed in micro laser heating of thin metal films and in laser surgery techniques [29–31]. Liu and Lu [32] and Lu et al. [33,34] reported that some thermal wave effects of changing power on bioheat transfer in tissue cannot be described by the Pennes' equation.

2.2. Hyperbolic heat equation

Since the experimental observation of a finite thermal wave speed in liquid helium [1], the fundamental wave behaviour in heat conduction has been argued from various physical view points [35–37]. The necessity of a finite heat propagation speed has also been demonstrated from a microscopic point of view [38,39]. Using the concept of a finite heat propagation velocity, Cattaneo [36] and Vernott [37] independently formulated a modified unsteady heat conduction equation, which is a linear extension of the unsteady Fourier equation, where additional τ_q is added to Eq. (1) in order to account for the thermal wave behaviour not captured by Fourier's theory:

$$q(\vec{r}, t+\tau_q) = -k\nabla T(\vec{r}, t) \tag{4}$$

where $\tau_q = \alpha/C_t^2$ is defined as the thermal relaxation time with α being the thermal diffusivity, and C_t being the speed of thermal wave in the medium [12,40]. The reciprocal of the relaxation time, $f = 1/\tau_q$, is the critical frequency above which the thermal wave behaviour occurs [38]. Since both τ_q and α are intrinsic thermal properties of the medium, the resulting thermal wave speed C_t is also an intrinsic property [41].

The first order Taylor expansion of (4) gives:

$$q(\vec{r}, t) + \tau_q \partial q(\vec{r}, t)/\partial t = -k\nabla T(\vec{r}, t) \tag{5}$$

Due to its similarity with the acoustic wave, the proposed wave-like propagation of thermal signals is termed the "second sound wave" [1,38].

A direct integration of (5) leads to [42]:

$$\int_0^t \left[q(\vec{r}, t) + \tau_q \partial q(\vec{r}, t)/\partial t\right] \mathrm{d}t = \int_0^t \left[-k\nabla T(\vec{r}, t)\right] \mathrm{d}t$$
$$\Rightarrow q(\vec{r}, t) = -\frac{k}{\tau_q}\exp\left(-\frac{t}{\tau_q}\right)\int_0^t \exp\left(\frac{t}{\tau_q}\right)\nabla T(\vec{r}, t)\,\mathrm{d}t \tag{6}$$

According to this equation, the heat flux $q(\vec{r}, t)$ at a certain time t depends on the entire history of the temperature gradient established from time 0 to t. In other words, the heat flux now has a memory that keeps track of the time-history of temperature gradient due to the appearance of τ_q [5,43]. The thermal wave theory ensures a strong path dependency for the temperature gradient rather than the point value depicted by Fourier's law [42,44].

2.2.1. Physical meaning and experimental determination of thermal relaxation time

Various physical points of view have been proposed for the physical meaning of thermal relaxation time τ_q [43]: τ_q results from the rate equation within the mainframe of the second law in non-equilibrium, irreversible thermodynamics; mechanically, τ_q arises due to the phase-lag between the heat-flux vector and temperature gradient in a high-rate response; when considering diffusion behaviour and wave propagation, τ_q is the physical constant at which the intrinsic length scales merge together.

The value of relaxation time for homogeneous materials can be calculated theoretically [45,46], which is, however, not suitable for materials having non-homogeneous inner structures such as skin tissue. There is, at present, no direct experimental method exists for determining τ_q. It has been suggested that τ_q can be determined by fitting experimental temperature data with theoretical predictions from the hyperbolic equation, by using τ_q as a variable parameter [47–51]. By using the equation, $\tau_q = \alpha/C_t^2$, τ_q for non-homogenous materials can also be determined based on the measurement of the thermal wave speed C_t, which can derived from the penetration time[1] and the distance of this point to the heat source, and the measurement of the thermal diffusivity α.

Kaminski [5] proposed that τ_q represents the interaction of different inner structural elements of material during heat transfer. For homogeneous materials, this interaction is at the molecular or crystal lattice level and τ_q has a value in the range of 10^{-8}–10^{-14} s. For heterogeneous materials, the structural heat transfer interaction takes place at a different size level and τ_q characterizes thermal inductance, defined as the time needed for accumulating the thermal energy required for propagative transfer between different elements internally. Accordingly, it may take a much larger

[1] The penetration time is the period between the appearance of the temperature jump (thermal wave front) and start of heating at a measurement point.

value (in the range of 10^{-3}–10^{3} s) in heterogeneous materials [52].

Most biological materials that contain cells, superstructures, liquids, and solid/soft tissue are non-homogeneous, resulting in higher thermal relaxation times compared to engineering materials. Vedavarz et al. [30] found that τ_q for some biological tissues lies in the range of 10–1000 s at cryogenic temperature and 1–100 s at room temperature. Brazhnikov et al. [49] and Kaminski [5] found $\tau_q = 20$–30 s for meat products; Mitra et al. [12] found that the τ_q for processed meat was about 15.5 s while Roetzel et al. [9] found it to be 1.77 s. As for skin tissue, no data about the thermal relaxation time has been reported although it has been determined for important cutaneous structures [53], and are detailed in Table 1. From the table we can see skin tissue has a "lengthy" relaxation time, which means it is desirable to develop a computational approach to examine the non-Fourier heat transfer process and the resulting mechanical response in skin tissue.

2.2.2. Thermal wave model of bioheat transfer

Substituting the bioheat conduction equation (2) into the thermal wave theory, Eq. (5), we can get thermal wave model of bioheat transfer:

$$\tau_q \rho c \frac{\partial^2 T}{\partial t^2} = k\nabla^2 T - \varpi_b \rho_b c_b T - (\tau_q \varpi_b \rho_b c_b + \rho c)\frac{\partial T}{\partial t} + \left(\varpi_b \rho_b c_b T_b + q_m + q_{ext} + \tau_q \frac{\partial q_m}{\partial t} + \tau \frac{\partial q_{ext}}{\partial t}\right) \tag{7}$$

The above equation is known as a hyperbolic bioheat equation because there appears a two double-derivative term (called the wave term) that modifies the parabolic Fourier heat equation [54] into a hyperbolic partial differential equation.

2.2.3. Application of the model

The above equation without blood perfusion terms was introduced by Luikov [52] to chemical and process engineering. It was subsequently advanced to heat transfer processes that take place in dissipative and dispersive systems where Fourier's heat equation fails to predict accurate temperatures. More details on the development of thermal wave theory in heat conduction can be found in Ozisik and Tzou [42].

Table 1
Thermal relaxation times of important cutaneous structures [53]

Structure	Size (μm)	Thermal relaxation time (approximate)
Melanosome	0.5–1	1 μs
Cell	10	300 μs
Blood vessel	50	1 ms
	100	5 ms
	200	20 ms

For biological materials, Mitra et al. [12] found that their experimental results can be well predicted by the hyperbolic heat conduction model. This model has also been applied to the measurement of blood perfusion rate [21,55,56], the prediction of temperature transients and thermal stresses in skin during cryopreservation [57], the prediction of temperature/thermal dose distributions in living tissue during thermal therapies [24], and the explanation of temperature oscillations [58].

The wave-like behaviour of bioheat transfer, occurring in skin tissue under different heating conditions, was studied by Liu et al. [16,59]: they compared the temperature and thermal damage distributions predicted separately by the thermal wave and Pennes models, and found they showed great deviation in all cases. They also found that, for heating with a high flux under an extremely short duration, the thermal wave model provides more realistic predictions. Similar results have also been reported by Ma et al. [60], who analyzed the non-Fourier effect of laser irradiation in human skin, and found that the rates of temperature rise at different depths of skin were comparatively slow due to the non-Fourier effect.

2.2.4. Problems with thermal wave model

Although the thermal wave model has explained many interesting phenomena [44] and the relaxation behaviour has been shown to be admissible within the framework of the second law of extended irreversible thermodynamics [43], its validity can be questionable. For example, it is not based on the details of energy transport in the material; material properties may not be regarded as constant, e.g. the relaxation time τ_q is generally temperature-dependent [43]; although the thermal wave model can capture the microscale response in time [40,42], the wave concept does not capture the microscale response in space [61,62] and the thermal wave model introduces some unusual physical solutions [46,63,64]; due to the assumption of a macroscopic behaviour averaged over many grains, the validity of the thermal wave model becomes debatable in view of the fast-transient response with microstructural interaction effects [65].

2.3. Dual-phase-lag (DPL) model

In order to account for deviations from the classical approach involving Fourier conduction and to consider the effect of microstructural interactions in the fast transient process of heat transport, an effect absent in the thermal wave model, a phase lag for temperature gradient, τ_T, is introduced [40,42,65]. Together with τ_q, the corresponding equation is called the dual-phase-lag (DPL) equation, and is stated as:

$$q(\vec{r}, t + \tau_q) = -k\nabla T(\vec{r}, t + \tau_T) \tag{8}$$

where τ_q and τ_T can be interpreted as periods arising from "thermal inertia" and "microstructural interaction",

respectively [66]: specifically, τ_q is the phase-lag in establishing the heat flux and associated conduction through a medium, while τ_T accounts for the diffusion of heat ahead of sharp wave fronts that would be induced by τ_q, and is the phase-lag in establishing the temperature gradient across the medium during which conduction occurs through its small-scale structures. Thus, Eq. (8) states that the gradient of temperature at a point in the material at time $t+\tau_T$ corresponds to the heat flux vector at the same point at time $t+\tau_q$ [67]. The Eq. (8) reduces to the thermal wave model by setting $\tau_T=0$ and reduces to Fourier's heat equation by also setting $\tau_q=0$.

Through the first and second order Taylor expansions, the DPL model can be developed into several pertinent models, which are now summarized.

2.3.1. Type 1 DPL model of bioheat transfer (DPL1MBT)

The simplest example of DPL model is its first order expansions for both q and T, given as:

$$q(\vec{r},t)+\tau_q\frac{\partial q(\vec{r},t)}{\partial t}=-k\left[\nabla T(\vec{r},t)+\tau_T\frac{\partial \nabla T(\vec{r},t)}{\partial t}\right] \tag{9}$$

Substituting the bioheat conduction equation (2) into this equation we obtain the so-called type 1 DPL model of bioheat transfer:

$$\begin{aligned}\tau_q\rho c\frac{\partial T^2}{\partial t^2}&=k\nabla^2T+\tau_Tk\nabla^2\frac{\partial T}{\partial t}-\varpi_b\rho_bc_bT\\&\quad-(\tau_q\varpi_b\rho_bc_b+\rho c)\frac{\partial T}{\partial t}\\&\quad+\left(\varpi_b\rho_bc_bT_a+q_{met}+q_{ext}+\tau_q\frac{\partial q_{met}}{\partial t}+\tau_q\frac{\partial q_{ext}}{\partial t}\right)\end{aligned} \tag{10}$$

The DPL1MBT model without blood perfusion terms has been shown to give good agreement with experiments across a wide range of length and time scales for engineering materials [66,68]. Antaki [15] pointed out that the DPL model combines the wave features of hyperbolic conduction with a diffusion-like feature not captured by the hyperbolic case. By fitting the experimental data of Mitra et al. [12] to the prediction of DPL1MBT without blood perfusion terms, it was found that $\tau_q=16$ s, $\tau_T=0.043$ s for experiment I[2] and $\tau_q=14$ s, $\tau_T=0.056$ s for experiment III.[3]

2.3.2. Type 2 DPL model of bioheat transfer (DPL2MBT)

Applying first-order and second-order Taylor series expansion for q and T, respectively, we have

$$q+\tau_q\frac{\partial q}{\partial t}=-k\left(\nabla T+\tau_T\frac{\partial\nabla T}{\partial t}+\frac{\tau_T^2}{2}\frac{\partial^2\nabla T}{\partial t^2}\right) \tag{11}$$

Substituting the bioheat conduction equation (2) into this equation we obtain the type 2 DPL model of bioheat transfer:

$$\begin{aligned}\tau_q\rho c\frac{\partial T^2}{\partial t^2}&=k\nabla^2T+\tau_Tk\nabla^2\frac{\partial T}{\partial t}+k\frac{\tau_T^2}{2}\frac{\partial^2}{\partial t^2}\nabla^2T\\&\quad-\varpi_b\rho_bc_bT-(\tau_q\varpi_b\rho_bc_b+\rho c)\frac{\partial T}{\partial t}\\&\quad+(\varpi_b\rho_bc_bT_a+q_{met}+q_{ext}+\tau_q\frac{\partial q_{met}}{\partial t}+\tau_q\frac{\partial q_{ext}}{\partial t})\end{aligned} \tag{12}$$

2.3.3. Type 3 DPL model of bioheat transfer (DPL3MBT)

Applying second-order Taylor series expansion for both q and T, respectively, we have

$$q+\tau_q\frac{\partial q}{\partial t}+\frac{\tau_q^2}{2}\frac{\partial^2q}{\partial t^2}=-k\left(\nabla T+\tau_T\frac{\partial\nabla T}{\partial t}+\frac{\tau_T^2}{2}\frac{\partial^2\nabla T}{\partial t^2}\right) \tag{13}$$

Substituting the bioheat conduction equation (2) into this equation we obtain the type 3 DPL model of bioheat transfer:

$$\begin{aligned}\frac{\tau_q^2}{2}\rho c\frac{\partial^3T}{\partial t^3}&=k\nabla^2T+k\tau_T\frac{\partial}{\partial t}\nabla^2T+k\frac{\tau_T^2}{2}\frac{\partial^2}{\partial t^2}\nabla^2T\\&\quad+(-\varpi_b\rho_bc_b)T+(-\tau_q\varpi_b\rho_bc_b-\rho c)\frac{\partial T}{\partial t}\\&\quad+\left(-\frac{\tau_q^2}{2}\varpi_b\rho_bc_b-\tau_q\rho c\right)\frac{\partial^2T}{\partial t^2}\\&\quad+\left(\varpi_b\rho_bc_bT_b+q_m+q_{ext}+\tau_q\frac{\partial q_m}{\partial t}+\tau_q\frac{\partial q_{ext}}{\partial t}\right.\\&\quad\left.+\frac{\tau_q^2}{2}\frac{\partial^2q_m}{\partial t^2}+\frac{\tau_q^2}{2}\frac{\partial^2q_{ext}}{\partial t^2}\right)\end{aligned} \tag{14}$$

3. Thermal damage

Presently, the Arrhenius burn integration, proposed by Henriques and Moritz [25,69], is widely used. They assert that skin damage can be represented as a chemical rate process, which is calculated by using a first-order Arrhenius rate equation, whereby damage is related to the rate of protein denaturation, k, and exposure time, t, at a given absolute temperature, T. The dimensionless measure of thermal damage, Ω, is introduced and its rate, k, is postulated to satisfy:

$$k(T)=\mathrm{d}\Omega/\mathrm{d}t=A\exp(-E_a/RT) \tag{15}$$

or, equivalently:

$$\Omega=\int_0^t A\exp(-E_a/RT)\,\mathrm{d}t \tag{16}$$

[2] The experiments were designed to show that heat waves take a finite time to reach a particular point inside the sample contrary to the instantaneous heat propagation as predicted by the Fourier model: two identical meat samples at different initial temperatures were brought into contact with each other.

[3] The experiments were designed to show wave superposition: one thin sample is sandwiched by two larger ones.

where A is a material parameter equivalent to a frequency factor, E_a is the activation energy, and $R = 8.314$ J/mol K is the universal gas constant. Eq. (15) indicates that a reaction proceeds faster with larger values of T or A for the same E_a, or with smaller values of E_a for the same A. The constants A and E_a are obtained experimentally.

In the study of Moritz and Henriques [25], the integration of (16) was carried out over the time range where the basal layer temperature was greater than or equal to 44 °C, which was the threshold temperature for thermal damage to skin. According to different levels of tissue damage and heating modes, Henriques [70] proposed different thresholds: (1) threshold A, the shortest time at which constant predetermined cutaneous surface temperature produces transepidermal necrosis (denoted by $\Omega = 1$); (2) threshold B, the longest time at which constant predetermined surface temperature could be tolerated without causing irreversible transepidermal injury (denoted by $\Omega = 0.53$); (3) threshold C, the shortest time at which cir-

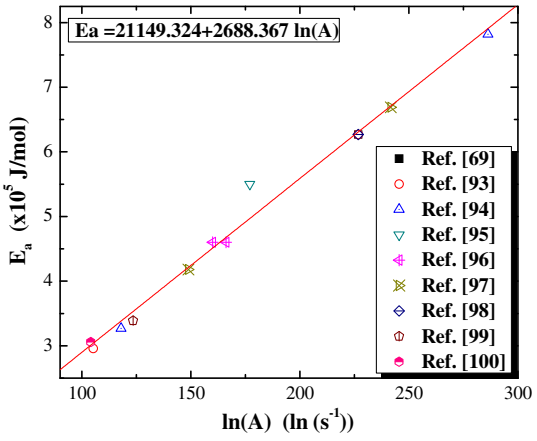

Fig. 2. Cross-plot of Arrhenius parameters (A, E_a) with regression fit (scattered points: values are taken from Refs. [69,93–100] which are indicated; line: best fit line by least squares).

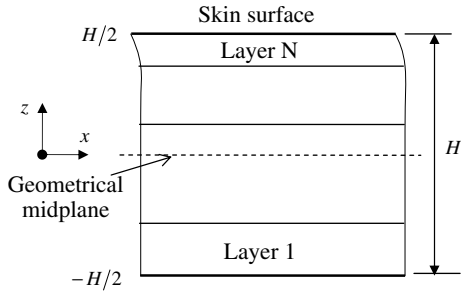

Fig. 3. Schematic of multi-layer skin for thermal stress analysis.

Table 2
Thermophysical properties of blood

Parameters		References
Blood density (kg/m^3)	1060.0	[84]
Blood specific heat (J/kg K)	3770.0	[85]
Arterial blood temperature (°C)	37	
Core temperature (°C)	37	

Table 3
Parameters for one-layer model

Parameters	Value	References
Thermal expansion coefficient λ ($\times 10^{-4}$/°C)	1	Assumption
Poisson's ratio (–)	0.48	[86]
Young's modulus (MPa) E	102	[87]
Skin density (kg/m^3)	1190.0	[84]
Skin thermal conductivity (W/m K)	0.235	[88]
Skin specific heat (J/kg K)	3600.0	[69]
Metabolic heat generation (W/m^3)	368.1	[89]
Thickness (m)	0.006	[90]

Table 4
Four-layer model

Parameters		Value	References
Thermal expansion coefficient ($\times 10^{-4}$/°C)	Stratum corneum	1	Assumption
	Epidermis	1	Assumption
	Dermis	1	Assumption
	Subcutaneous fat	1	Assumption
Poisson's ratio (–)	Stratum corneum	0.48	[86]
	Epidermis	0.48	[86]
	Dermis	0.48	[86]
	Subcutaneous fat	0.48	[86]
Young's modulus (MPa)	Stratum corneum	1998.0	[87]
	Epidermis	102	[87]
	Dermis	10.2	[87]
	Subcutaneous fat	0.0102	[87]
Skin density (kg/m^3)	Stratum corneum	1500.0	[84]
	Epidermis	1190.0	[84]
	Dermis	1116.0	[84]
	Subcutaneous fat	971.0	[84]
Skin thermal conductivity (W/m K)	Stratum corneum	0.235	
	Epidermis	0.235	[88]
	Dermis	0.445	[88]
	Subcutaneous fat	0.185	[69]
Skin specific heat (J/kg K)	Stratum corneum	3600.0	
	Epidermis	3600.0	[69]
	Dermis	3300.0	[69]
	Subcutaneous fat	2700.0	[69]
Metabolic heat generation (W/m^3)	Stratum corneum	368.1	
	Epidermis	368.1	[89]
	Dermis	368.1	[89]
	Subcutaneous fat	368.3	[89]
Thickness (m)	Stratum corneum	0.00002	Assumption
	Epidermis	0.00008	Assumption
	Dermis	0.0015	[91]
	Subcutaneous fat	0.0044	Assumption

cumambient and circumradiant heat of measured intensity caused transepidermal necrosis.

Many researchers have proposed other models, but most of them have similar format, where the only differences are in the coefficients used in the burn damage integral, arising from the different experimental databases used to define the models and the different emphasis when analysing the burn process. The available Arrhenius parameters (A, E_a) used to calculate thermal damage for skin tissue from the literature has been reviewed, and is fitted with the method used by Wright [71], as shown in Fig. 2. The results of Fig. 2 clearly suggest a linear relationship after a least-square fit between the Arrhenius parameters for skin tissue, given by:

$$E_a = 21149.324 + 2688.367 \ln(A) \tag{17}$$

It should be noted here that the coefficients A and E_a are determined from experimental measurements based on the first-order Arrhenius rate equation (15), which involves a local skin temperature. This means that the experiments used to determine these parameters must account for the hyperbolic conduction so that they can be used in the context of hyperbolic heat conduction (as done in the later part of this paper) [72, 73]. However, there is no such data available in the literature and hence the test data from Fig. 2 are used in this study although they are based on the Fourier heat conduction.

With the Eq. (17), the reaction rate of the thermal damage process follows as:

$$k(T) = \exp[(E_a - 21149.324)/2688.367] \exp(-E_a/RT) \tag{18}$$

If the temperature is constant and E_a specified, the thermal damage can be calculated as:

$$\Omega = \int_0^t k(T)\,\mathrm{d}t = k(T)t \tag{19}$$

Assuming that $\Omega = 1.0$ denotes the beginning of irreversible damage, we can calculate the time for the appearance of irreversible damage at temperature T as specified by threshold A, as:

$$t_{\Omega=1} = 1/k(T) = 1/(\exp[(E_a - 21149.324)/2688.367] \exp(-E_a/RT)) \tag{20}$$

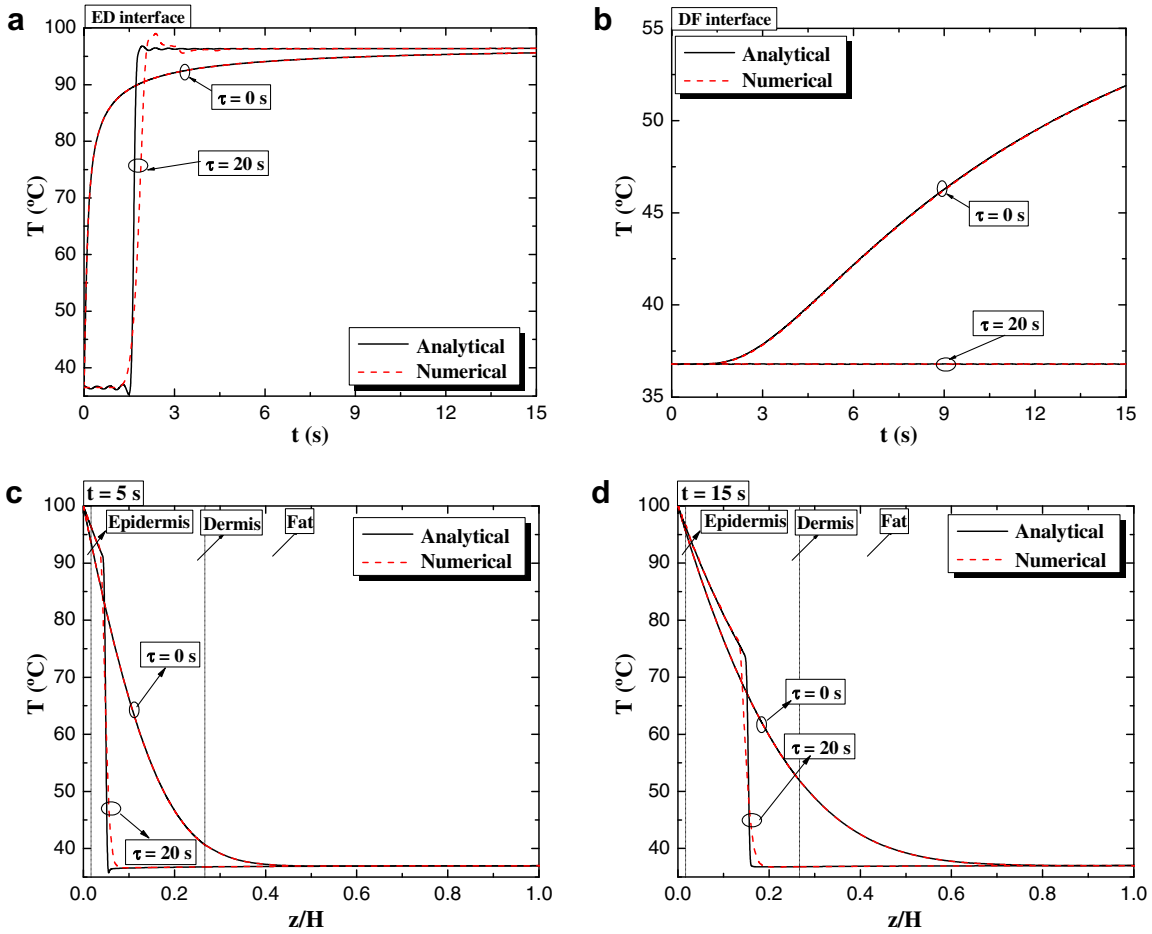

Fig. 4. Verification of numerical model for temperature results: (a) variation with time at ED interface; (b) variation with time at DF interface; (c) distribution along skin depth at $t = 5$ s; (d) distribution along skin depth at $t = 15$ s.

4. Thermal stresses

As previously discussed, skin has a complicated multi-layer structure (see Fig. 1a). Whilst the thermal properties of the layers have the same order of magnitude, see Table 4, so that a one-layer continuum model for heat transfer may be assumed, the mechanical properties vary greatly by up to three orders of magnitude from one layer to another. Consequently, in order to obtain the distribution of heat-induced stresses, the skin must be treated as a laminated composite structure, with each layer assumed to be uniform with linear, orthotropic thermoelastic properties, as shown in Fig. 3. The thermomechanical behaviour of skin tissue is simplified to be a 'sequentially-coupled' problem, in other words, the mechanical behaviour has no influence on thermal behaviour and vice versa. The temperature field in skin tissue is first obtained from solving the governing equations of biological heat transfer, which is then used as the input to the thermomechanical model, from which the corresponding thermal stress field is obtained. Note that the skin surface is positioned at $z = H/2$, where H is the thickness of skin and z is measured from the mid-plane of skin structure.

Details of the derivation procedures for thermal stress distributions in skin layers have been reported elsewhere [74]. For brevity, only the closed form solutions are presented here. The in-plane stresses parallel to the skin surface in each layer (Fig. 3) can be obtained as:

$$\{\sigma_{xx}\}_k = \overline{E}_k \left\{ \begin{array}{l} -\bar{\lambda}_k \Delta T + \left[C_a(1+v_k)\left(\sum_{i=1}^{M} \int_{z_{i-1}}^{z_i} \overline{E}_i \bar{\lambda}_i \Delta T \, dz \right) \right. \\ \left. + C_b(1+v_k)\left(\sum_{i=1}^{M} \int_{z_{i-1}}^{z_i} \overline{E}_i \bar{\lambda}_i \Delta T z \, dz \right) \right] \\ + z(1+v_k)\left[C_b\left(\sum_{i=1}^{M} \int_{z_{i-1}}^{z_i} \overline{E}_i \bar{\lambda}_i \Delta T \, dz \right) \right. \\ \left. + C_d(1+v_k)\left(\sum_{i=1}^{M} \int_{z_{i-1}}^{z_i} \overline{E}_i \bar{\lambda}_i \Delta T z \, dz \right) \right] \end{array} \right\} \tag{21}$$

where C_a, C_b, C_d are material constants that depend on the relative thickness of each layer [74], $\overline{E} = E/(1-v^2)$, and $\bar{\lambda} = (1+v)\lambda$; E, v and λ are the Young's modulus, Poisson ratio and linear coefficient of thermal expansion, respectively.

The above method is applied to single-layer skin model and multi-layer skin model, respectively. The solutions are summarized below.

(1) *One-layer model*

$$\sigma_{xx}(x,t) = -\overline{E}\bar{\lambda}(T - T_0) + \frac{\overline{E}\bar{\lambda}}{H}\int_{-H/2}^{H/2}(T - T_0)\,dz + \overline{E}\bar{\lambda}\frac{12x}{H}\int_{-H/2}^{H/2}(T - T_0)z\,dz \tag{22}$$

(2) *Four-layer model (stratum corneum–living epidermis–dermis–fat)*

$$\sigma_{xx} = (1+v_f)\overline{E}_f \times \left\{ \begin{array}{l} \left[(a'_{11}+a'_{12})\left(\int_{z_0}^{z_1} \overline{E}_f\bar{\lambda}_f \Delta T\,dz + \int_{z_1}^{z_2} \overline{E}_d\bar{\lambda}_d \Delta T\,dz + \int_{z_2}^{z_3} \overline{E}_e\bar{\lambda}_e \Delta T\,dz + \int_{z_3}^{z_4} \overline{E}_{sc}\bar{\lambda}_{sc}\Delta T\,dz \right) \right. \\ \left. + (b'_{11}+b'_{12})\left(\int_{z_0}^{z_1} \overline{E}_f\bar{\lambda}_f \Delta T z\,dz + \int_{z_1}^{z_2} \overline{E}_d\bar{\lambda}_d \Delta T z\,dz + \int_{z_2}^{z_3} \overline{E}_e\bar{\lambda}_e \Delta T z\,dz + \int_{z_3}^{z_4} \overline{E}_{sc}\bar{\lambda}_{sc}\Delta T z\,dz \right) \right] \\ + z\left[(b'_{11}+b'_{12})\left(\int_{z_0}^{z_1} \overline{E}_f\bar{\lambda}_f \Delta T\,dz + \int_{z_1}^{z_2} \overline{E}_d\bar{\lambda}_d \Delta T\,dz + \int_{z_2}^{z_3} \overline{E}_e\bar{\lambda}_e \Delta T\,dz + \int_{z_3}^{z_4} \overline{E}_{sc}\bar{\lambda}_{sc}\Delta T\,dz \right) \right. \\ \left. + (d'_{11}+d'_{12})\left(\int_{z_0}^{z_1} \overline{E}_f\bar{\lambda}_f \Delta T z\,dz + \int_{z_1}^{z_2} \overline{E}_d\bar{\lambda}_d \Delta T z\,dz + \int_{z_2}^{z_3} \overline{E}_e\bar{\lambda}_e \Delta T z\,dz + \int_{z_3}^{z_4} \overline{E}_{sc}\bar{\lambda}_{sc}\Delta T z\,dz \right) - \lambda_f \Delta T \right] \end{array} \right\} \tag{23}$$

$z_0 \leqslant z < z_1$, Fat layer

$$\sigma_{xx} = (1+v_d)\overline{E}_d \times \left\{ \begin{array}{l} \left[(a'_{11}+a'_{12})\left(\int_{z_0}^{z_1} \overline{E}_f\bar{\lambda}_f \Delta T\,dz + \int_{z_1}^{z_2} \overline{E}_d\bar{\lambda}_d \Delta T\,dz + \int_{z_2}^{z_3} \overline{E}_e\bar{\lambda}_e \Delta T\,dz + \int_{z_3}^{z_4} \overline{E}_{sc}\bar{\lambda}_{sc}\Delta T\,dz \right) \right. \\ \left. + (b'_{11}+b'_{12})\left(\int_{z_0}^{z_1} \overline{E}_f\bar{\lambda}_f \Delta T z\,dz + \int_{z_1}^{z_2} \overline{E}_d\bar{\lambda}_d \Delta T z\,dz + \int_{z_2}^{z_3} \overline{E}_e\bar{\lambda}_e \Delta T z\,dz + \int_{z_3}^{z_4} \overline{E}_{sc}\bar{\lambda}_{sc}\Delta T z\,dz \right) \right] \\ + z\left[(b'_{11}+b'_{12})\left(\int_{z_0}^{z_1} \overline{E}_f\bar{\lambda}_f \Delta T\,dz + \int_{z_1}^{z_2} \overline{E}_d\bar{\lambda}_d \Delta T\,dz + \int_{z_2}^{z_3} \overline{E}_e\bar{\lambda}_e \Delta T\,dz + \int_{z_3}^{z_4} \overline{E}_{sc}\bar{\lambda}_{sc}\Delta T\,dz \right) \right. \\ \left. + (d'_{11}+d'_{12})\left(\int_{z_0}^{z_1} \overline{E}_f\bar{\lambda}_f \Delta T z\,dz + \int_{z_1}^{z_2} \overline{E}_d\bar{\lambda}_d \Delta T z\,dz + \int_{z_2}^{z_3} \overline{E}_e\bar{\lambda}_e \Delta T z\,dz + \int_{z_3}^{z_4} \overline{E}_{sc}\bar{\lambda}_{sc}\Delta T z\,dz \right) \right] - \lambda_d \Delta T \end{array} \right\} \tag{24}$$

$z_1 \leqslant z < z_2$, Dermis layer

$$\sigma_{xx} = (1+v_e)\overline{E}_e \times \left\{ \begin{array}{l} \left[\begin{array}{l} (a'_{11}+a'_{12})\left(\int_{z_0}^{z_1}\overline{E}_f\bar{\lambda}_f\Delta T\,dz + \int_{z_1}^{z_2}\overline{E}_d\bar{\lambda}_d\Delta T\,dz + \int_{z_2}^{z_3}\overline{E}_e\bar{\lambda}_e\Delta T\,dz + \int_{z_3}^{z_4}\overline{E}_{sc}\bar{\lambda}_{sc}\Delta T\,dz\right) \\ +(b'_{11}+b'_{12})\left(\int_{z_0}^{z_1}\overline{E}_f\bar{\lambda}_f\Delta Tz\,dz + \int_{z_1}^{z_2}\overline{E}_d\bar{\lambda}_d\Delta Tz\,dz + \int_{z_2}^{z_3}\overline{E}_e\bar{\lambda}_e\Delta Tz\,dz + \int_{z_3}^{z_4}\overline{E}_{sc}\bar{\lambda}_{sc}\Delta Tz\,dz\right) \end{array} \right] \\ +z\left[\begin{array}{l} (b'_{11}+b'_{12})\left(\int_{z_0}^{z_1}\overline{E}_f\bar{\lambda}_f\Delta T\,dz + \int_{z_1}^{z_2}\overline{E}_d\bar{\lambda}_d\Delta T\,dz + \int_{z_2}^{z_3}\overline{E}_e\bar{\lambda}_e\Delta T\,dz + \int_{z_3}^{z_4}\overline{E}_{sc}\bar{\lambda}_{sc}\Delta T\,dz\right) \\ +(d'_{11}+d'_{12})\left(\int_{z_0}^{z_1}\overline{E}_f\bar{\lambda}_f\Delta Tz\,dz + \int_{z_1}^{z_2}\overline{E}_d\bar{\lambda}_d\Delta Tz\,dz + \int_{z_2}^{z_3}\overline{E}_e\bar{\lambda}_e\Delta Tz\,dz + \int_{z_3}^{z_4}\overline{E}_{sc}\bar{\lambda}_{sc}\Delta Tz\,dz\right) \end{array} \right] - \lambda_e\Delta T \end{array} \right\} \quad (25)$$

$z_2 \leqslant z < z_3$, Epidermis layer

$$\sigma_{xx} = (1+v_{sc})\overline{E}_{sc} \times \left\{ \begin{array}{l} \left[\begin{array}{l} (a'_{11}+a'_{12})\left(\int_{z_0}^{z_1}\overline{E}_f\bar{\lambda}_f\Delta T\,dz + \int_{z_1}^{z_2}\overline{E}_d\bar{\lambda}_d\Delta T\,dz + \int_{z_2}^{z_3}\overline{E}_e\bar{\lambda}_e\Delta T\,dz + \int_{z_3}^{z_4}\overline{E}_{sc}\bar{\lambda}_{sc}\Delta T\,dz\right) \\ +(b'_{11}+b'_{12})\left(\int_{z_0}^{z_1}\overline{E}_f\bar{\lambda}_f\Delta Tz\,dz + \int_{z_1}^{z_2}\overline{E}_d\bar{\lambda}_d\Delta Tz\,dz + \int_{z_2}^{z_3}\overline{E}_e\bar{\lambda}_e\Delta Tz\,dz + \int_{z_3}^{z_4}\overline{E}_{sc}\bar{\lambda}_{sc}\Delta Tz\,dz\right) \end{array} \right] \\ +z\left[\begin{array}{l} (b'_{11}+b'_{12})\left(\int_{z_0}^{z_1}\overline{E}_f\bar{\lambda}_f\Delta T\,dz + \int_{z_1}^{z_2}\overline{E}_d\bar{\lambda}_d\Delta T\,dz + \int_{z_2}^{z_3}\overline{E}_e\bar{\lambda}_e\Delta T\,dz + \int_{z_3}^{z_4}\overline{E}_{sc}\bar{\lambda}_{sc}\Delta T\,dz\right) \\ +(d'_{11}+d'_{12})\left(\int_{z_0}^{z_1}\overline{E}_f\bar{\lambda}_f\Delta Tz\,dz + \int_{z_1}^{z_2}\overline{E}_d\bar{\lambda}_d\Delta Tz\,dz + \int_{z_2}^{z_3}\overline{E}_e\bar{\lambda}_e\Delta Tz\,dz + \int_{z_3}^{z_4}\overline{E}_{sc}\bar{\lambda}_{sc}\Delta Tz\,dz\right) \end{array} \right] - \lambda_{sc}\Delta T \end{array} \right\} \quad (26)$$

$z_3 \leqslant z < z_4$, Stratum corneum layer

In these equations, the subscripts "sc", "e", "d" and "f" denote stratum corneum, epidermis, dermis and fat layer, respectively.

5. Solutions

5.1. Analytical solutions for one-layer skin model

With closed-form solution of temperature of thermal wave model under boundary condition $\begin{cases} T = T_\infty, z = 0 \\ \partial T/\partial z = 0, z = H \end{cases}$ and initial condition $\begin{cases} T = T_i, t = 0 \\ \partial T/\partial t = 0, t = 0 \end{cases}$ obtained by Liu et al. [16], and analytical solution of thermal stress as obtained in Section 4, the corresponding closed-form solution of stress can be obtained as: when $\left|1 - \frac{\tau_q \rho_b \omega_b c_b}{\rho c}\right| < \frac{(2n-1)\pi\sqrt{\alpha\tau}}{H}$ when $\left|1 - \frac{\tau_q \rho_b \omega_b c_b}{\rho c}\right| > \frac{(2n-1)\pi\sqrt{\alpha\tau}}{H}$

$$\sigma_{xx}(z,t) = \text{term1} \times \text{term2} + \text{term3} \quad (27)$$

$$\text{term1} = \overline{E}\bar{\lambda}\left(T_\infty - T_i - \frac{Q_r}{\rho_b\omega_b c_b}\right) \Big/ \cosh\left(\sqrt{\frac{\rho_b\omega_b c_b}{k}}H\right) \quad (28)$$

$$\text{term2} = -\cosh\left[\sqrt{\frac{\rho_b\omega_b c_b}{k}}(z-H)\right] + \left\{ \frac{\left[\sqrt{\frac{k}{\rho_b\omega_b c_b}}\sinh\left(\sqrt{\frac{\rho_b\omega_b c_b}{k}}H\right)\right]}{H} \times \frac{12(H/2-z)}{H}\left(\begin{array}{l} \sqrt{\frac{k}{\rho_b\omega_b c_b}}\frac{H}{2}\sinh\left(\sqrt{\frac{\rho_b\omega_b c_b}{k}}H\right) \\ +\frac{k}{\rho_b\omega_b c_b}\left[1-\cosh\left(\sqrt{\frac{\rho_b\omega_b c_b}{k}}H\right)\right] \end{array} \right) \right\} \quad (29)$$

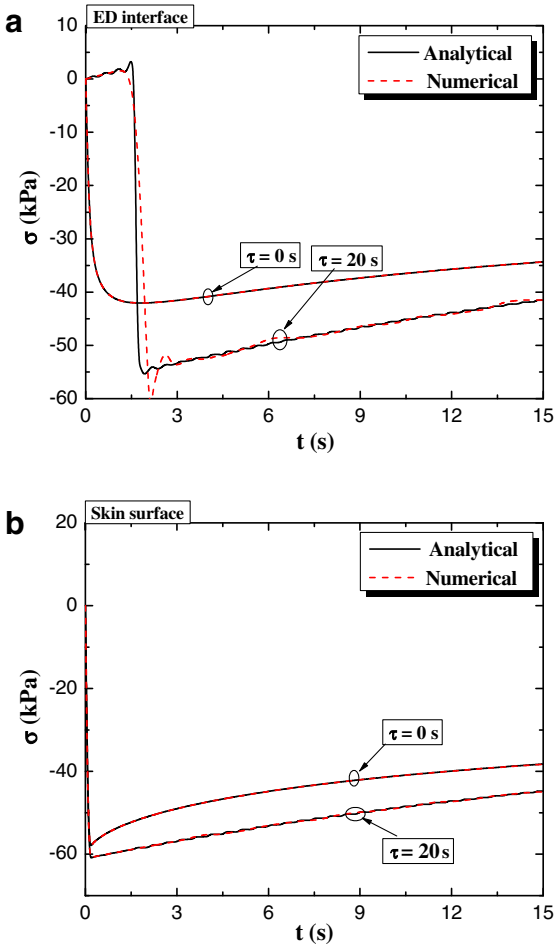

Fig. 5. Verification of numerical model for thermal stress results: (a) variation with time at skin surface; (b) variation with time at ED interface.

$$\text{term3} = \overline{E\lambda} e^{-(\alpha'/2)t} \times \sum_{n=1}^{\infty} \left\{ \begin{array}{l} (A_n \cos \varpi_n t + B_n \sin \varpi_n t) \\ \left\{ \begin{array}{l} -\sin\left(\frac{(n-\frac{1}{2})\pi}{H} z\right) + \frac{1}{(n-0.5)\pi} \\ + \frac{12(H/2-z)}{H} \left(\frac{H^2}{(2n-1)\pi} - \left(\frac{H}{(n-0.5)\pi}\right)^2 \sin(n\pi - 0.5\pi) \right) \end{array} \right\} \end{array} \right\} \tag{30}$$

$$\sigma_{xx}(z,t) = \text{term1} \times \text{term2} + \text{term3} \tag{31}$$

$$\text{term1} = \overline{E\lambda} \left(T_\infty - T_i - \frac{Q_r}{\rho_b \omega_b c_b} \right) \Big/ \cosh\left(\sqrt{\frac{\rho_b \omega_b c_b}{k}} H \right) \tag{32}$$

$$\text{term2} = -\cosh\left[\sqrt{\frac{\rho_b \omega_b c_b}{k}} (z - H) \right] + \frac{\left[\sqrt{\frac{k}{\rho_b \omega_b c_b}} \sinh\left(\sqrt{\frac{\rho_b \omega_b c_b}{k}} H \right) \right]}{H} \times \frac{12(H/2-z)}{H} \left(\begin{array}{l} \sqrt{\frac{k}{\rho_b \omega_b c_b}} \frac{H}{2} \sinh\left(\sqrt{\frac{\rho_b \omega_b c_b}{k}} H \right) \\ + \frac{k}{\rho_b \omega_b c_b} \left[1 - \cosh\left(\sqrt{\frac{\rho_b \omega_b c_b}{k}} H \right) \right] \end{array} \right) \tag{33}$$

$$\text{term3} = \overline{E\lambda} e^{-(\alpha/2)t} \times \sum_{n=1}^{\infty} \left\{ \begin{array}{l} [C_n \exp(\gamma_n t) + D_n \exp(-\gamma_n t)] \\ \left\{ \begin{array}{l} -\sin\left(\frac{(n-\frac{1}{2})\pi}{H} z\right) + \frac{1}{(n-0.5)\pi} + \\ \frac{12(H/2-z)}{H} \left(\frac{H^2}{(2n-1)\pi} - \left(\frac{H}{(n-0.5)\pi}\right)^2 \sin(n\pi - 0.5\pi) \right) \end{array} \right\} \end{array} \right\} \tag{34}$$

where skin surface is at $z = 0$.

These closed-form solutions of temperature and thermal stress can be used to check the accuracy of predictions using numerical tools.

5.2. Numerical solutions

Since the structure of skin is very complicated and cannot normally be treated as a single homogeneous layer, the finite difference method is used to solve Eqs. (3), (7), (12), (14) and (16). Once the temperature profiles are obtained, the corresponding thermal stresses can be calculated from

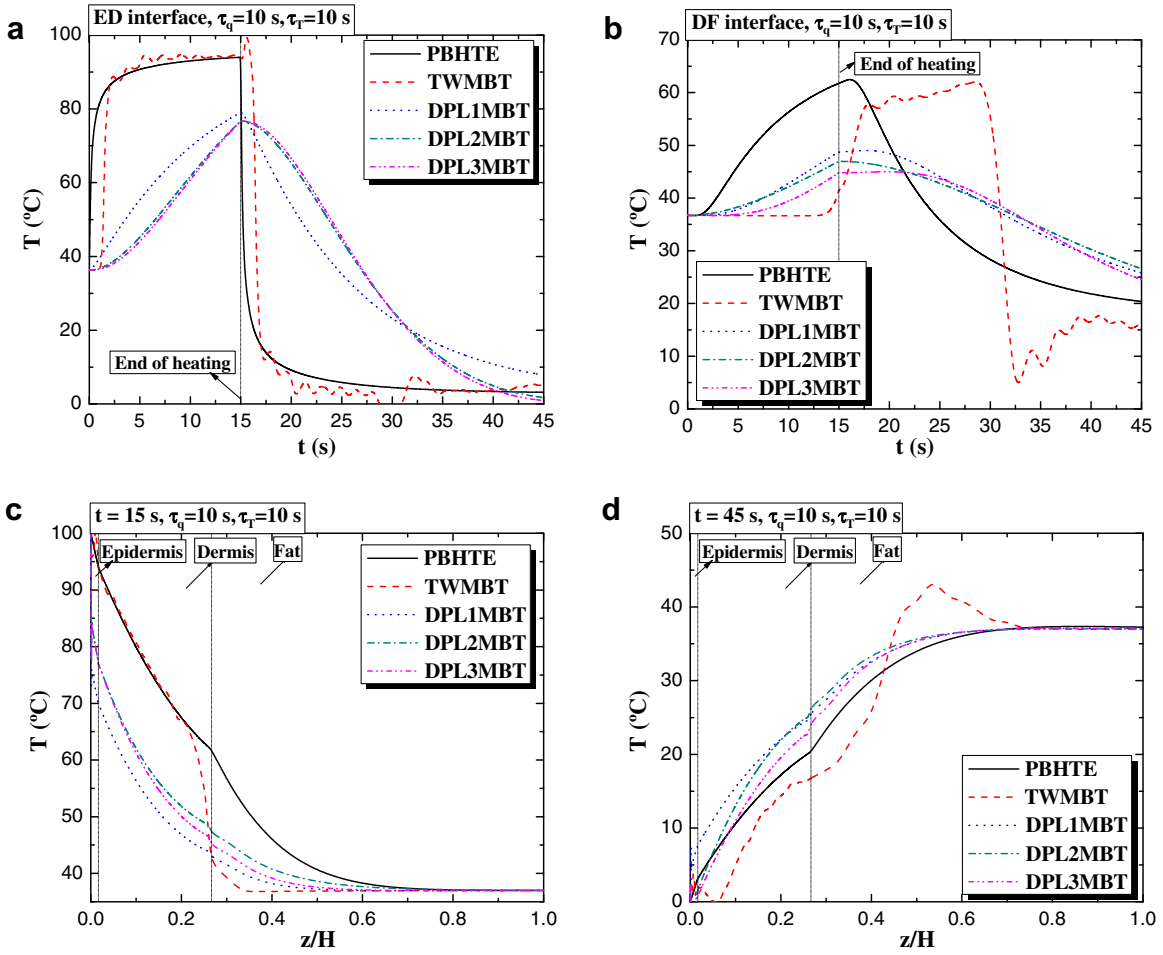

Fig. 6. Comparison of predictions of temperature from different models: (a) variation with time at ED interface; (b) variation with time at DF interface; (c) distribution along skin depth at $t = 15$ s; (d) distribution along skin depth at $t = 45$ s (PBHTE: Pennes model; TWMBT: thermal wave model; DPL: dual-phase lag model).

the analytical results for multi-layer skin model, given in Eqs. (23)–(26).

6. Case study

6.1. Description of the problem

The skin is initially cooled by natural convection using environmental air ($T_e = 25$ °C, $h = 7$ W/m^2 K). At $t = 0$, the skin surface is suddenly taken into contact with a hot source of constant temperature 100 °C such as boiling water; after contacting for 15 s, the hot source is removed and the skin is cooled by use of water ice mixture of 0 °C for 30 s.

6.1.1. Treatment of skin

According to the real structure of skin (Fig. 1a), the skin is modeled as a layered structure, as shown in Fig. 1b. For the heat transfer process, the skin is divided into three layers with different properties: epidermis with thickness of 0.1 mm, dermis with thickness of 1.5 mm, and subcutaneous fat with thickness of 4.4 mm. Blood perfusion is only considered in the dermis layer while metabolic heat generation is considered in all three layers. For the thermal stress calculation, our previous study [75] and other studies [76,77] have shown that the thin stratum corneum plays an important role in skin thermomechanical behaviour due to its comparatively large Young's modulus and cannot be ignored; thus, the four-layer skin model is adopted. The relevant parameters used for both heat transfer and thermal stress analyses are summarized in Tables 2–4.

6.1.2. Calculation of burn injury

The skin burn injury is calculated using the burn integration of (19), with the frequency factor $A = 3.1 \times 10^{98}$ and the ratio of activation energy to universal gas constant $E_a/R = 75{,}000$ (see [70]).

6.2. Results and discussion

The above problem is solved by using different models: Pennes model, thermal wave model and three types of

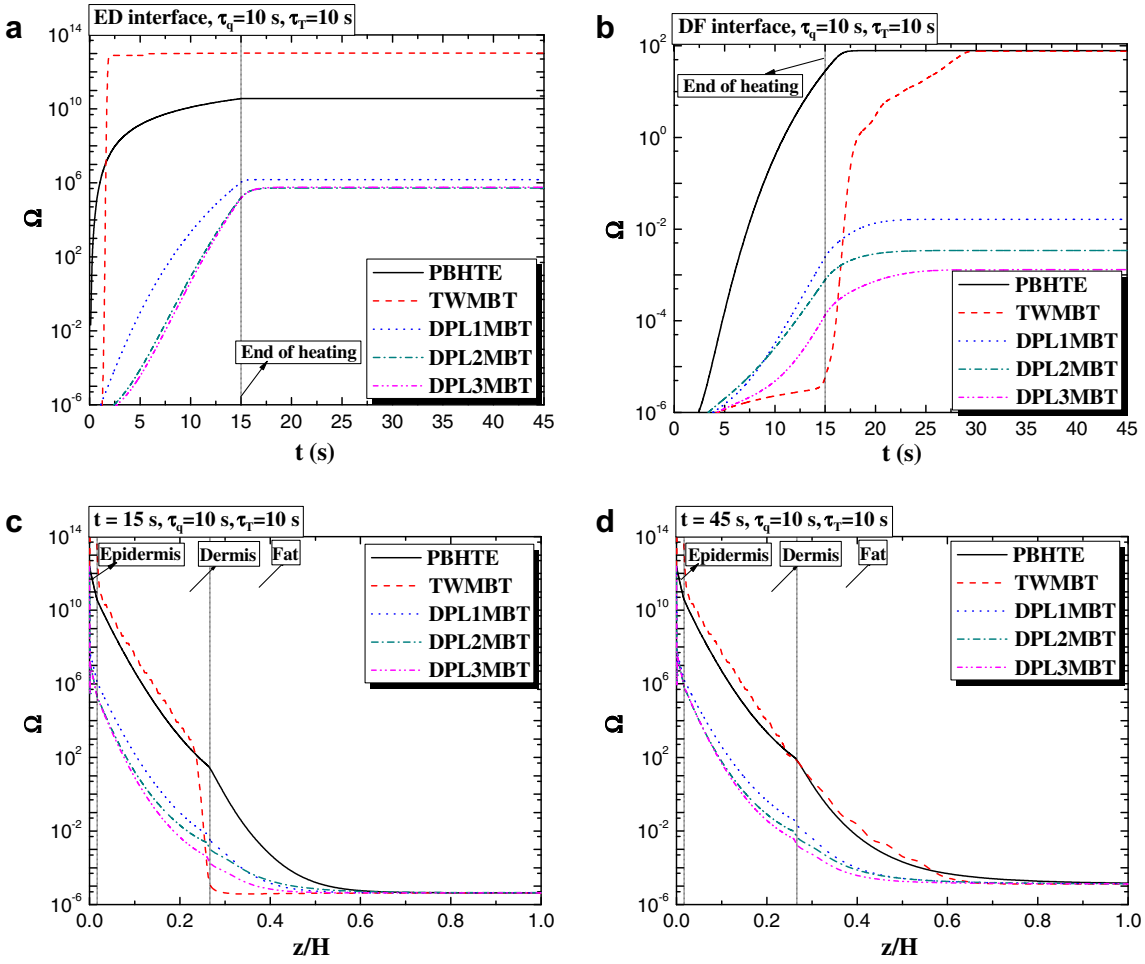

Fig. 7. Comparison of predictions of thermal damage from different models: (a) variation with time at ED interface; (b) variation with time at DF interface; (c) distribution along skin depth at $t = 15$ s; (d) distribution along skin depth at $t = 45$ s (PBHTE: Pennes model; TWMBT: thermal wave model; DPL: dual-phase lag model).

dual-phase lag models (DPL1MBT, DPL2MBT and DPL3MBT). The results and discussion are given in the following sections.

6.2.1. Verification of numerical model

For one-layer skin model, Figs. 4 and 5 compare the analytical and numerical predictions. The results demonstrate excellent agreement for both temperature and stress fields; more details of the numerical approach are described below.

6.2.2. Comparison of different bioheat transfer models

For the multi-layer skin model, the comparison between predictions of different bioheat transfer models is shown in Fig. 6 for temperature, in Fig. 7 for thermal damage, and in Fig. 8 for thermal stress. The temperature, thermal damage and thermal stress distributions in the skin at the end of heating ($t = 15$ s) and cooling ($t = 45$ s) are shown separately in in Figs. 6c–d, 7c–d and 8c–d, whilst Figs. 6a, b and 7a, b plot the corresponding temperature and burn damage at the ED interface and DF interface as functions of time, respectively. Since the nociceptors emerge from superficial dermal nerve plexuses running beneath the epidermis into epidermis [78] as low as 50 μm from the skin surface [79], attention is focused on thermal stress at the skin surface and ED interface, as shown in Fig. 8a and b.

The results of Fig. 6a–d demonstrate that tissue temperature calculated from different bioheat transfer models can deviate substantially under constant surface temperature heating. With the thermal wave model, the tissue temperature inside the body was undisturbed during the initial stage of heating before jumping instantaneously (Fig. 6b); this may be viewed as the wave front emerging from the finite propagation of the thermal wave or the existence of the relaxation time τ_q. The unchanged tissue temperature initially may be attributed to the nonthermally consumption related biological activities [16]. The results from the three DPL models exhibit similar behaviours, and all differ from the results of both Pennes model and thermal wave model. Unlike thermal wave model, no wave behaviour is observed in the DPL models as expected, but a non-Fourier diffusion-like behaviour exists due to

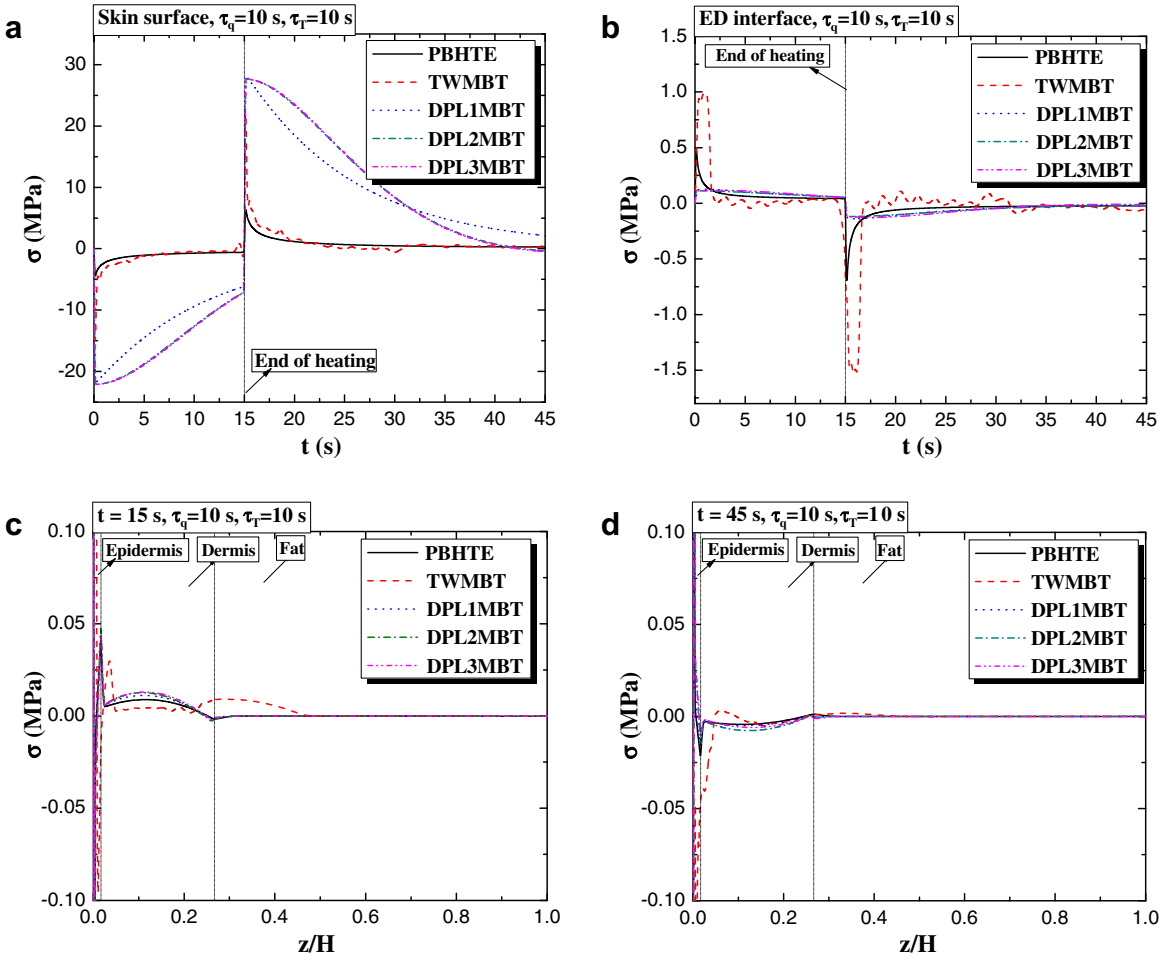

Fig. 8. Comparison of predictions of thermal stress from different models: (a) variation with time at skin surface; (b) variation with time at ED interface; (c) distribution along skin depth at $t = 15$ s; (d) distribution along skin depth at $t = 45$ s (PBHTE: Pennes model; TWMBT: thermal wave model; DPL: dual-phase lag model).

the second thermal relaxation time τ_T whose effect is to weaken the thermal wave, thereby destroying the sharp wave front. It is noticed that a sudden temperature drop for heating or a step for cooling at the skin surface is associated with the DPL models, as shown in Fig. 6c and d. It should be noted that there is a cross over of the solution beyond $t = 33$ s between the solutions of DPL1MBT, DPL2MBT and DPL3MBT. This is because in the DPL1MBT, the surrounding temperature is higher than those of DPL2MBT and DPL3MBT, as can be seen from Fig. 6d, which results in the slower decrease of temperature at the ED interface. Another interesting phenomenon is the increase of temperature at the DF interface after $t = 32$ s. This is attributed to the wave front feature of the thermal wave model. During the cooling process, the cooling thermal wave front arrives at the DF interface at about $t = 32$ s, causing a sudden decrease of the temperature to a very low value, as can be seen from Fig. 6b. After that, the DF interface is heated by the surrounding tissue at a higher temperature. Similar phenomenon can also be observed in Fig. 9b.

There is a reason that the various orders of τ_T and τ_q may yield close results, and the authors are encouraged to provide mathematical/numerical reasoning for it. The "closeness" of the DPL solutions can be explained mathematically. Eqs. (9), (11), (13) can be rewritten as:

$$\begin{aligned}&\sum_{n=0}^{\infty}\frac{\tau_q^n}{n!}\frac{\partial q^n(\vec{r},t)}{\partial t^n} = -k\left(\sum_{m=0}^{\infty}\frac{\tau_T^m}{m!}\frac{\partial \nabla T^m(\vec{r},t)}{\partial t^m}\right)\\ &\Rightarrow \sum_{n=0}^{\infty}\frac{\partial q^n(\vec{r},t)}{\partial([(n!)^{1/n}t]}/\tau_q)^n = -k\left(\frac{\partial q^m(\vec{r},t)}{\partial([(m!)^{1/m}t]}/\tau_T)^m\right)\end{aligned} \tag{35}$$

In view of the finite-difference approximations, effect of τ_T will become important if t is much smaller than τ_T and effect of τ_T^m will become important if $[(m!)^{1/m}t]^m$ is much smaller than τ_T^m. Depending on the value of τ_T and the accuracy demanded, the former condition may or may not imply the latter. Exemplified by the last two terms on the right-hand-side of Eq. (11) with *constant* τ_T and τ_q:

$$\begin{aligned}&q + \frac{\partial q}{\partial(t/\tau_q)} + \frac{\partial^2 q}{\partial\left(\sqrt{2}t/\tau_q\right)^2}\\ &\quad = -K\left(\nabla T + \frac{\partial \nabla T}{\partial(t/\tau_T)} + \frac{\partial^2 \nabla T}{\partial\left(\sqrt{2}t/\tau_T\right)^2}\right)\end{aligned} \tag{36}$$

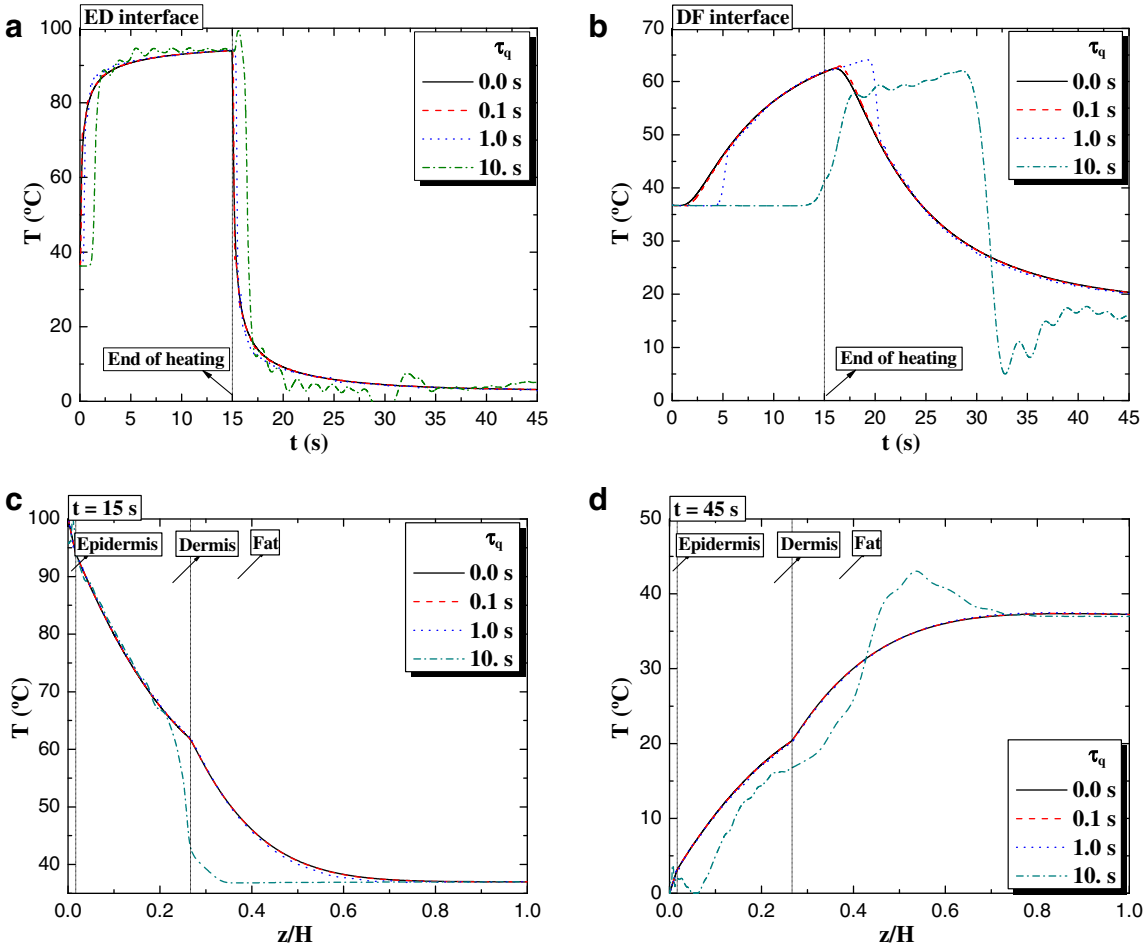

Fig. 9. Influence of thermal relaxation time τ_q on temperature from thermal wave model: (a) variation with time at ED interface; (b) variation with time at DF interface; (c) distribution along skin depth at $t = 15$ s; (d) distribution along skin depth at $t = 45$ s.

The large differences amongst the predicted temperatures between the models can cause significant deviations in burn evaluations. For example, the thermal damage predicted by thermal wave model at the end of heating for the ED interface is the largest, about three orders larger in magnitude than that from Pennes model and about seven orders larger than those from DPL models. A wave front for thermal damage is also observed for thermal wave model, which appears in Fig. 7b as a steep profile. As for the thermal damage distribution along the skin depth, Pennes model and thermal wave model give similar results, which are much larger in magnitude than those from DPL models.

Although the thermal stresses developed due to non-uniform temperature distributions are confined near the surface, see Fig. 8c and d, both the skin surface and ED interface are subjected to large tensile stresses, >10 MPa, see Fig. 8a and b, during both heating and cooling processes. This implies higher thermal damage occurring in these locations, consistent with the results of Fig. 7a and b. Note that the large tensile stresses predicted by the multi-layer skin model are in sharp contrast with those obtained with the one-layer model, Fig. 5. Furthermore, the magnitude of stress at the skin surface obtained with the DPL models is much larger than that with other models, although the same boundary condition is applied. This is caused by the sudden temperature drop at skin surface, Fig. 6c.

The mean mechanical threshold of nociceptors in the skin is in the range of about 0–0.6 MPa and mainly between 0.1 and 0.2 MPa [80]. Our results (Fig. 8a and b) show that the thermal stress is significantly larger than the threshold for all the three different kinds of models. This clearly indicates that, in addition to heating, thermal stress may also contribute to thermal pain. Other supporting evidence shows that, for the same level of nociceptor activity, a heat stimulus evokes more pain than a mechanical stimulus, and that the deformation of tissue due to heating and cooling may explain the origins of pain [81,82].

6.2.3. Thermal wave model of bioheat transfer

The calculation with the thermal wave model has been carried out for four different cases, where $\tau_q = 0.0$, 0.1, 1.0, and 10.0 s, with $\tau_q = 0$ corresponding to the Pennes model. The skin temperature distribution at the end of heating, $t = 15$ s, and cooling, $t = 45$ s, is shown separately in Fig. 9a and b, while Fig. 9c and d plot the corresponding temperature profiles at the ED and DF interfaces,

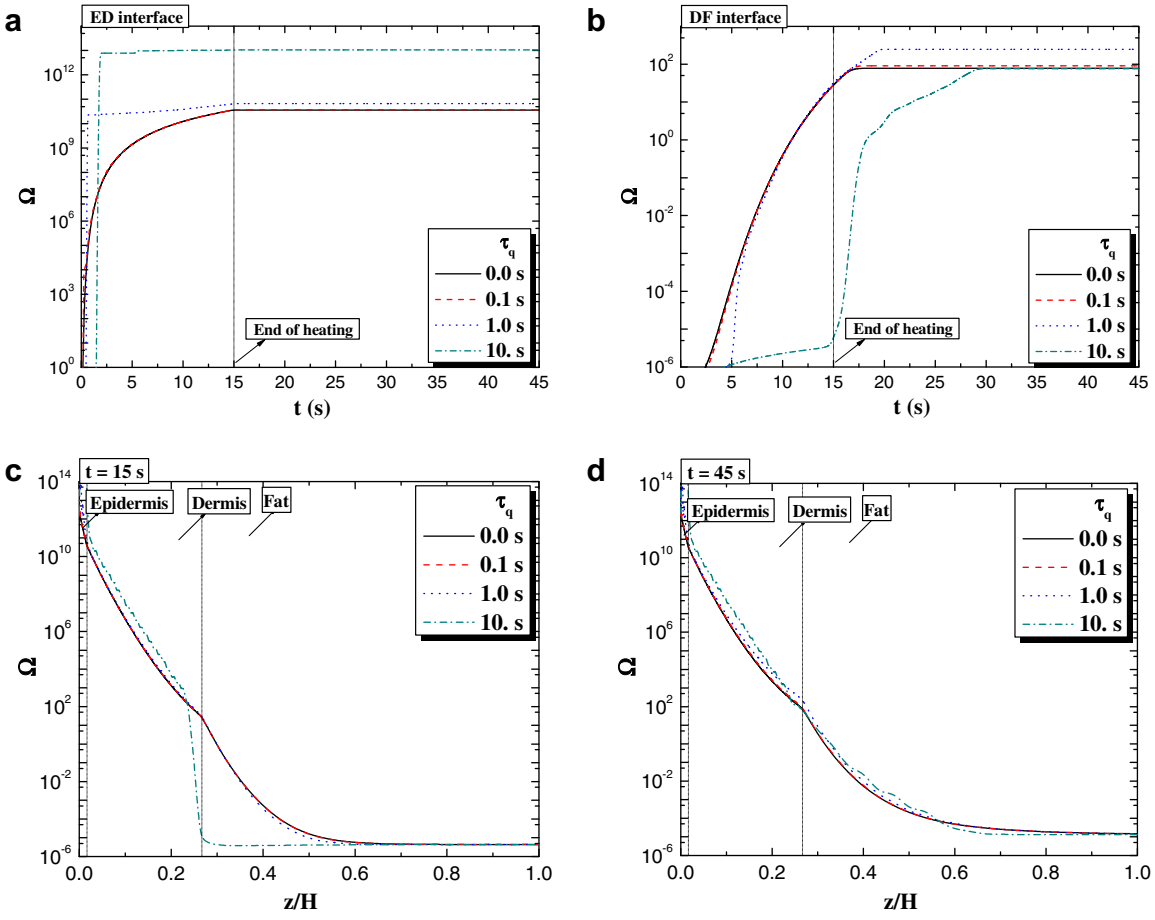

Fig. 10. Influence of τ_q on thermal damage results from thermal wave model: (a) variation with time at ED interface; (b) variation with time at DF interface; (c) distribution along skin depth at $t = 15$ s; (d) distribution along skin depth at $t = 45$ s.

respectively. Skin thermal damage and thermal stress are plotted in Figs. 10a–d and 11a–d, respectively.

As shown in Fig. 9a and b, the thermal relaxation time τ_q tends to induce an abrupt step in the temperature, introducing a wave-front, which separates the heated surface area from the unheated inner area. As it appears, when $\tau_q > 1.0$ s, the magnitude of τ_q has an important effect on temperature prediction and, thus, on thermal damage and thermal stress evaluations; conversely it makes little difference when $\tau_q \leqslant 0.$ s. This can be easily observed from the temperature history at the DF interface, as shown in Fig. 9(b). The appearance of the wave front for $\tau_q = 1.0$ s occurs at $t \approx 5$ s, while for $\tau_q = 10$ s it occurs much later at $t \approx 14$ s. Since the thermal wave speed C_t is correlated with τ_q from $C_t = \sqrt{\alpha/\tau_q}$, a smaller τ_q leads to a larger C_t for a fixed α with α being the thermal diffusivity.

A wave-like behaviour can also be observed in the results of thermal damage. For example, at the ED interface, little or no damage appears before $t \approx 3$ s for $\tau_q = 10$ s, whilst a sudden jump happens thereafter and the resulting damage is about three orders larger than the cases when τ_q is smaller. However, there is almost no thermal damage at the DF interface during the entire heating process.

Thermal stress output shows a similar behaviour except for the peak values, where a larger τ_q results in a higher peak. Once again, the value is larger than the threshold of nociceptors.

6.2.4. Dual-phase-lag model of bioheat transfer

Since different DPL models give similar results, as shown above, onlythe first model, DPL1MBT, is discussed here. The calculation of DPL1MBT has been carried out for nine cases: $\tau_q = 0.1$, 1.0, 10.0 s and $\tau_T = 0.1$, 1.0, 10.0 s; for comparison, the results corresponding to the case $\tau_q = \tau_T = 0$ are also included. The results for temperature distributions are presented in Figs. 12–15. The trends of thermal damage and thermal stresses are similar to those exhibited by temperature and hence, for brevity, are not included below.

6.2.5. Effect of τ_q

The effect of τ_q on temperature evolution at $\tau_T = 0.1$ s is shown in Fig. 12. Note that the results are similar to those of thermal wave model, especially for smaller τ_q: obvious wave-fronts can be observed, and the wave-front at the

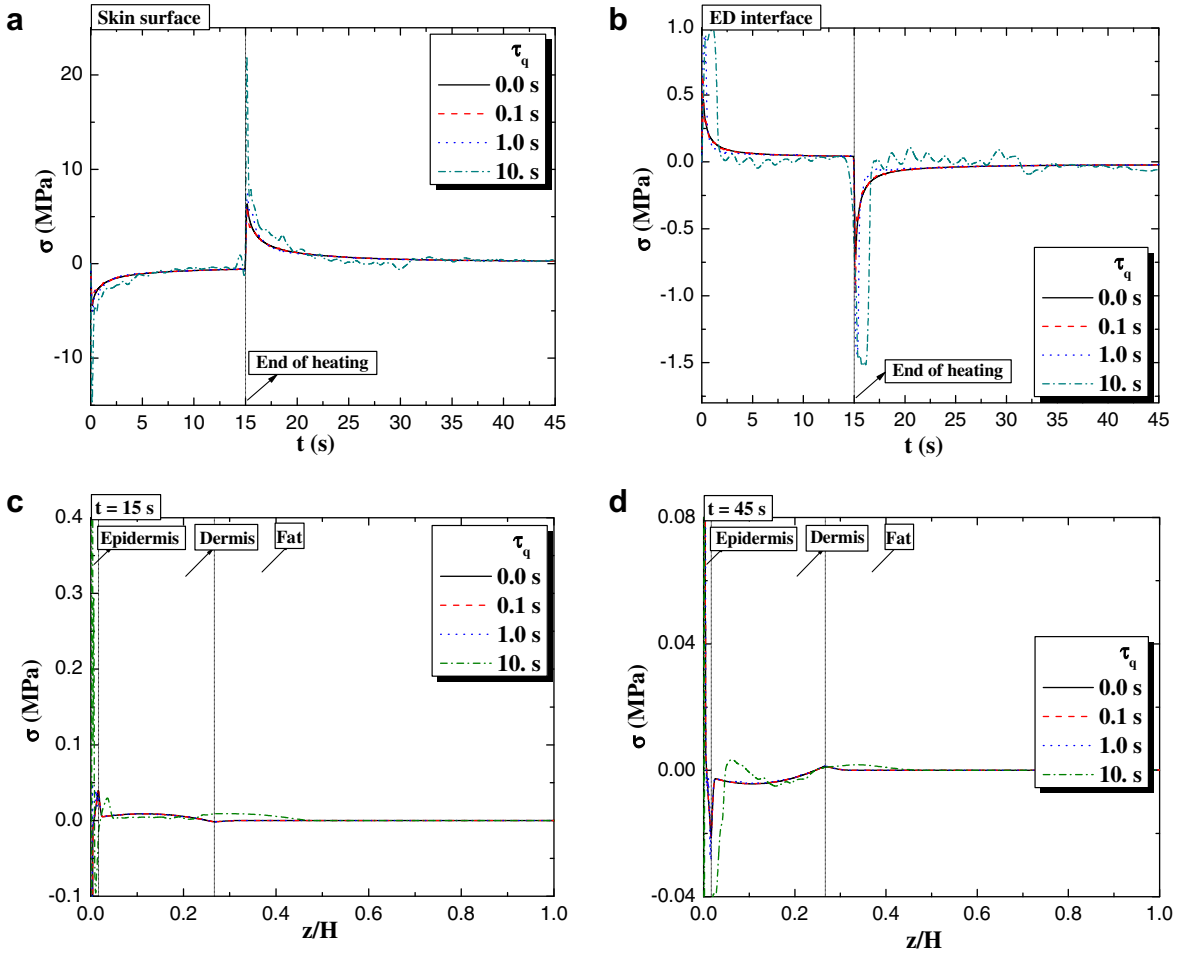

Fig. 11. Influence of τ_q on thermal stress results from thermal wave model: (a) variation with time at skin surface; (b) variation with time at ED interface; (c) distribution along skin depth at $t = 15$ s; (d) distribution along skin depth at $t = 45$ s.

same place appears earlier for a smaller value of τ_q. With increasing τ_q, the temperature is generally lower during initial heating but higher during cooling.

6.2.6. Effect of τ_T

The effects of τ_T on temperature profile are given in Fig. 13 for $\tau_q = 0.1$ s and in Fig. 14 for $\tau_q = 10$ s.

As can be seen from Fig. 13, no obvious wave-fronts can be found, which is attributable to the stronger dissipation from the mixed derivative term ($\tau_T k \nabla^2 \partial T/\partial t$), as shown in Eq. (12). The results are almost the same for different values of τ_T, except for $\tau_T = 10.0$ s where the temperature is lower during initial heating but higher under cooling.

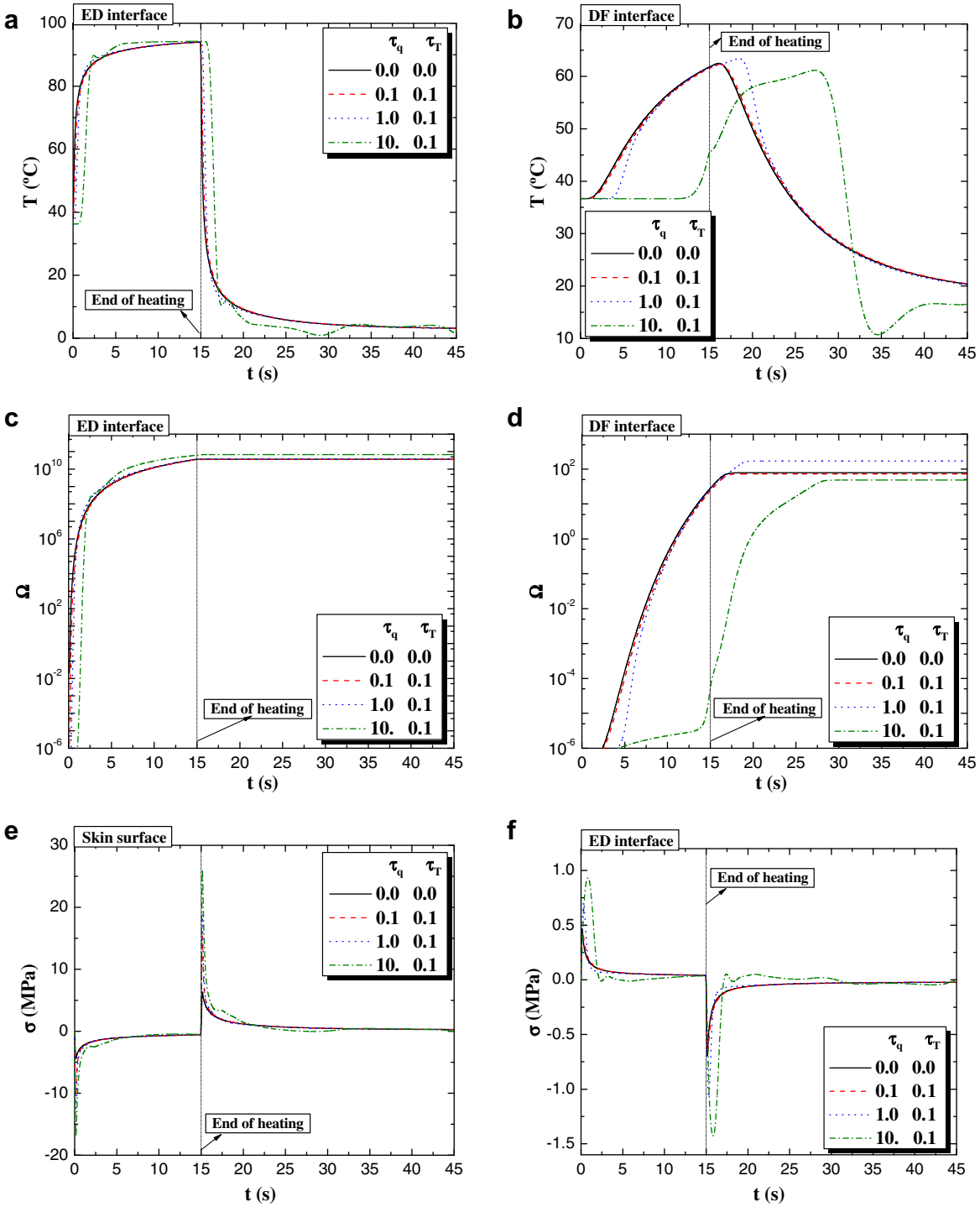

Fig. 12. Influence of τ_q on temperature results from type I dual-phase lag model (DPL1MBH) at $\tau_T = 0.1$ s: (a) temperature variation with time at ED interface; (b) temperature variation with time at DF interface; (c) thermal damage variation with time at ED interface; (d) thermal damage variation with time at DF interface; (e) thermal stress variation with time at skin surface: (f) thermal stress variation with time at ED interface.

When $\tau_q = 10.0$ s, as shown in Fig. 14, a wave behaviour is observed for all cases in spite of the different values of τ_T, which demonstrates that τ_q, rather than τ_T, dominates the mechanism of thermal wave propagation in skin tissue. However, the sharp wave-fronts due to τ_q are smoothed by the promoting conduction of τ_T, and the effect is more noticeable with increasing values of τ_T, leading to the non-Fourier diffusion-like conduction. This result agrees well with the non-Fourier behaviour observed for engineering materials [31,40,62]. However, despite different values of τ_q, the absolute value of thermal stress for $\tau_T = 10.0$ s is much larger at skin surface but much lower at ED inter-

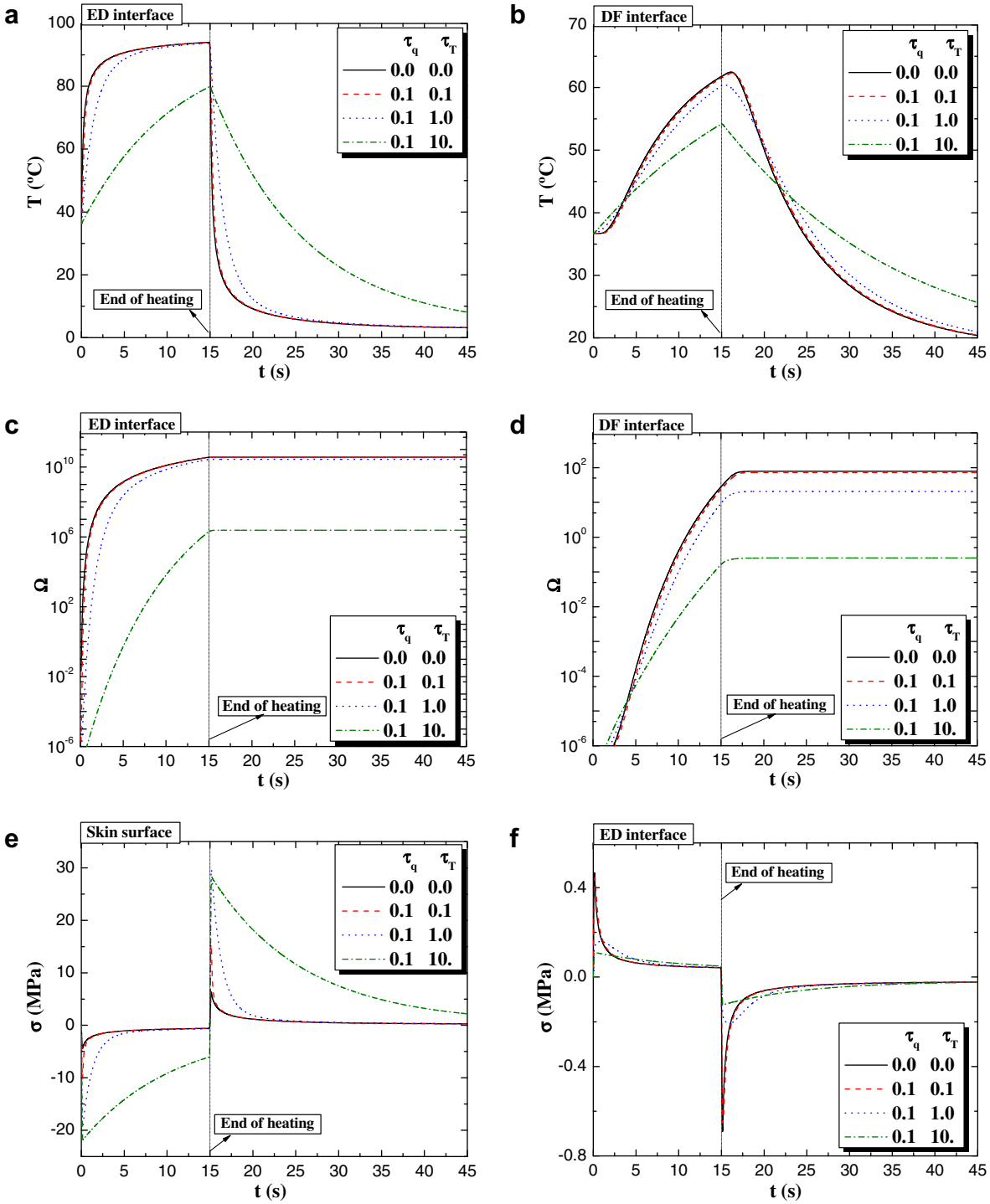

Fig. 13. Influence of τ_T on temperature results from type I dual-phase lag model (DPL1MBH) at $\tau_q = 0.1$ s: (a) temperature variation with time at ED interface; (b) temperature variation with time at DF interface; (c) thermal damage variation with time at ED interface; (d) thermal damage variation with time at DF interface; (e) thermal stress variation with time at skin surface; (f) thermal stress variation with time at ED interface.

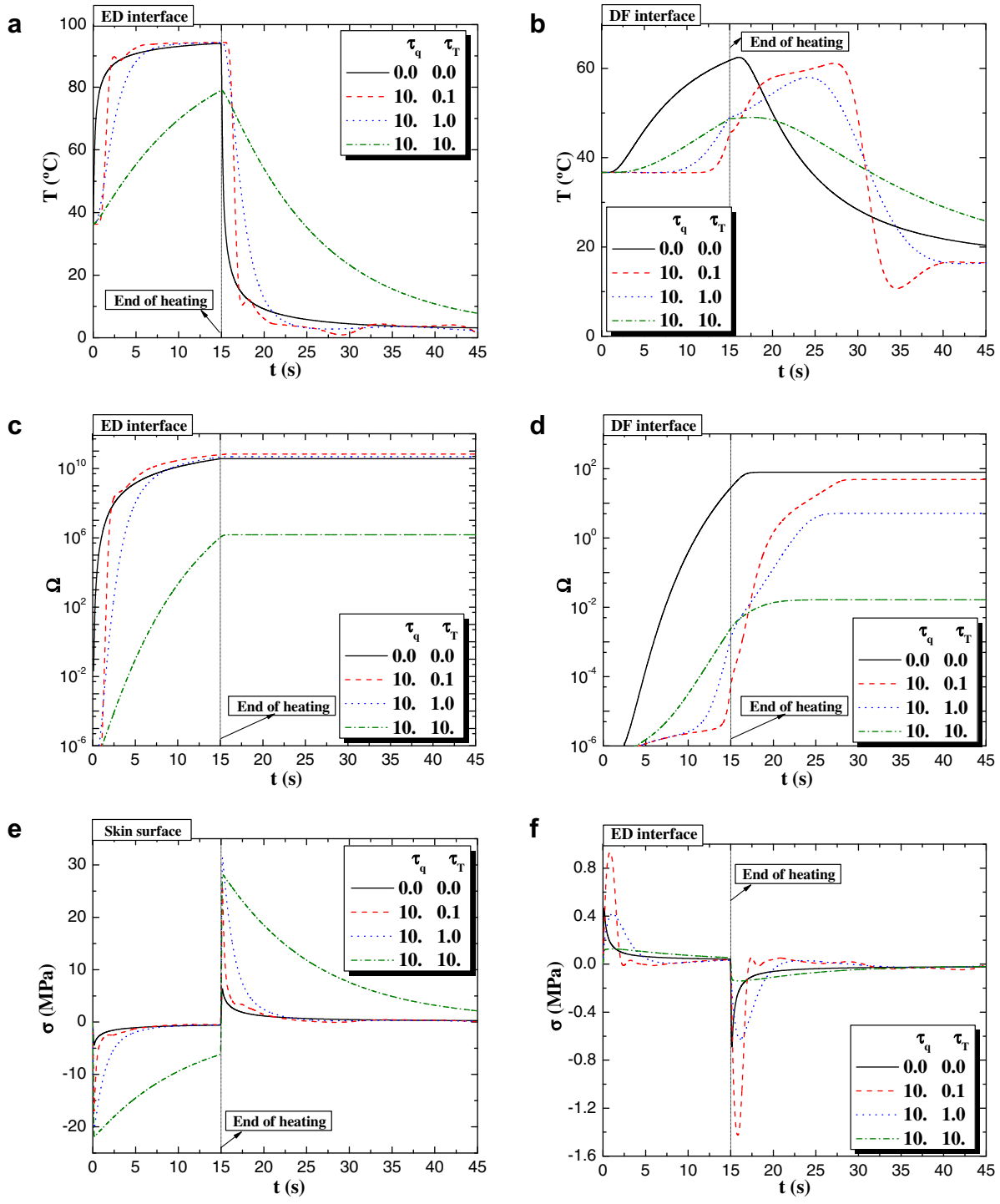

Fig. 14. Influence of τ_T on temperature results from type I dual-phase lag model (DPL1MBH) at $\tau_q = 10.0$ s: (a) temperature variation with time at ED interface; (b) temperature variation with time at DF interface; (c) thermal damage variation with time at ED interface; (d) thermal damage variation with time at DF interface; (e) thermal stress variation with time at skin surface; (f) thermal stress variation with time at ED interface.

face (not shown here for brevity). This arises because the thermal stress is influenced by temperature change along the whole skin depth, as shown in Eq. (23).

6.2.7. Effect of τ_q/τ_T

Tzou [40] has suggested that the ratio τ_q/τ_T dominates the lagging behaviour of heat transfer, i.e., the thermal responses are identical for a specified value of τ_q/τ_T. To check the suitability of this assertion in the cases here, comparisons of temperature distributions under the same τ_q/τ_T ratio are performed for three different cases, $\tau_q/\tau_T = 0.1, 1.0, 10$, as shown in Fig. 15. It is clear, from our results that there is no concurrency of behaviour for temperature, as well as thermal damage and thermal stress,

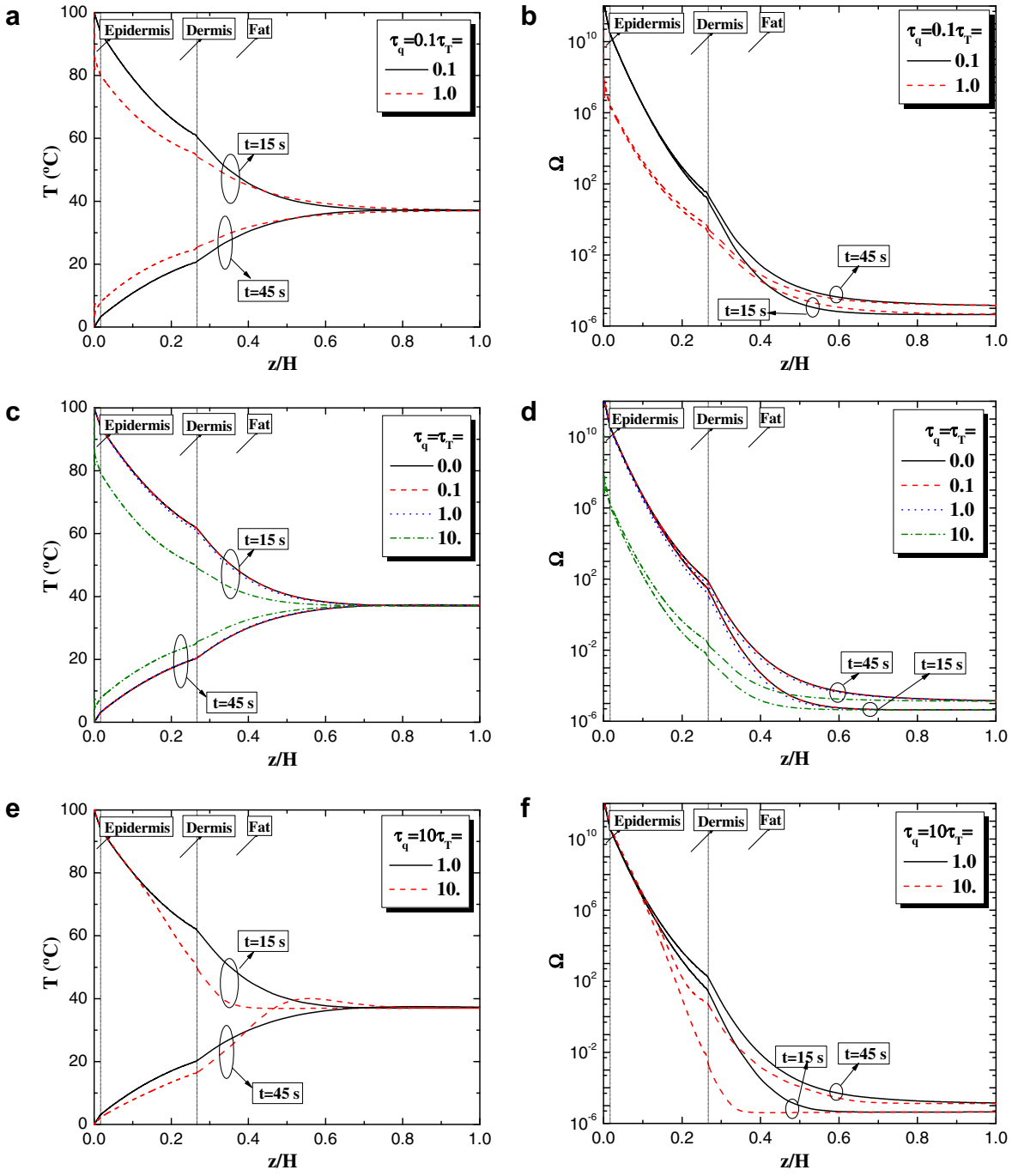

Fig. 15. Influence of ratios of τ_T/τ_q on predictions of temperature for type I dual-phase lag model (DPL1MBH): (a) variation with time at ED interface and DF interface for $\tau_T/\tau_q = 0.1$; (b) distribution along skin depth for $\tau_T/\tau_q = 0.1$; (c) variation with time at ED interface and DF interface for $\tau_T/\tau_q = 1.0$; (d) distribution along skin depth for $\tau_T/\tau_q = 1.0$; (e) variation with time at ED interface and DF interface for $\tau_T/\tau_q = 10.0$; (f) distribution along skin depth for $\tau_T/\tau_q = 10.0$.

in the three cases studied, which implies that the lagging thermomechanical behaviour in skin tissue depends on the absolute magnitudes of τ_T and τ_q, in addition to the ratio of τ_q/τ_T. A similar conclusion has been obtained for engineering materials [83]. The difference between our and Tzou's observations are due to the different problems tackled. Tzou [40] derived analytically the thermal lagging behaviour in a semi-infinite solid without instantaneous surface heating, which is different from the problems tackled in this work. The tangling behaviour of the real and apparent heat sources in our work as shown in Eq. (10), for example, may very well yield a lagging temperature that depends on the individual values of τ_T and τ_q rather than their ratio.

7. Conclusions

The thermal relaxation time for biological tissue is typically large, leading to the non-Fourier thermal behaviour of bioheat transfer. In this paper, the dual-phase-lag model is employed to study bioheat transfer in skin tissue, for it has the ability to characterize microstructural interactions in heat transport. Together with the Thermal Wave model of bioheat transfer, the non-Fourier thermo-mechanical behaviour of skin tissue is analyzed under surface heating boundary conditions. Exact solutions for temperature, thermal stress and thermal damage fields for single-layer skin model were presented. For multilayer models, to counter the mathematical difficulties induced by the mixed spatial and time derivatives and blood perfusion terms, numerical simulations with the finite difference method were used. The main conclusions are: (1) substantial discrepancies exist among the predictions by PBHTE, TWMBT and DPLMBT whilst different DPL models give similar results; (2) both types of relaxation time, τ_T and τ_q, have a significant influence on the temperature, thermal damage and thermal stress fields; (3) it is τ_q, not τ_T, which dominates the thermal wave propagation, with τ_q inducing a sharp wave-front that is smoothed by τ_T; (4) under the conditions studied in the paper, it is the absolute magnitudes of τ_T and τ_q, not the ratio τ_q/τ_T, which decides the thermomechanical behaviour of skin tissue; (5) in addition to heating/cooling, skin thermal stresses may also contribute to thermal pain.

Our results demonstrate that non-Fourier feature may play an important role in thermal behaviour of skin tissue in some cases. However, no such experiments have been performed hitherto and there is no reported data of the exact relaxation times of skin tissue. Further experimental verification is therefore necessary to measure the transport of energy in living systems at the micro-scale level, from which detailed data on relaxation times of tissue may be obtained. Besides, it should be pointed out that, in the analysis hitherto, it has been assumed that the thermal and mechanical properties of the skin layers are constant, i.e., independent upon thermal denaturation (shrinkage, damage). Existing test data on the effects of temperature and damage on the physical properties of skin are scarce, and will be the subject of future studies.

Acknowledgements

This work is supported by the Overseas Research Studentship (ORS) and Overseas Trust Scholarship of Cambridge University, the National Natural Science Foundation of China (10328203, 10572111, 10632060), the National 111 Project of China (B06024), and the National Basic Research Program of China (2006CB601202).

References

[1] V. Peshkov, Second sound in helium II, J. Phys. VIII 381 (1944).
[2] J.B. Brown, D.Y. Chung, P.W. Matthews, Heat pulse at low temperature, Phys. Rev. Lett. 21 (1966) 241.
[3] D.E. Glass, M.N. Ozisik, B. Vick, Hyperbolic heat conduction with surface radiation, Int. J. Heat Mass Transfer 28 (10) (1985) 1823–1830.
[4] A. Banerjee, A.A. Ogale, C. Das, K. Mitra, C. Subramanian, Temperature distribution in different materials due to short pulse laser irradiation, Heat Transfer Eng. 26 (8) (2005) 41–49.
[5] W. Kaminski, Hyperbolic heat conduction equation for materials with a nonhomogeneous inner structure, J. Heat Transfer, Trans. ASME 112 (3) (1990) 555–560.
[6] A. Grassmann, F. Peters, Experimental investigation of heat conduction in wet sand, Heat Mass Transfer/Waerme- und Stoffuebertragung 35 (4) (1999) 289–294.
[7] H. Herwig, K. Beckert, Experimental evidence about the controversy concerning Fourier or non-Fourier heat conduction in materials with a nonhomogeneous inner structure, Heat Mass Transfer/Waerme- und Stoffuebertragung 36 (5) (2000) 387–392.
[8] H. Herwig, K. Beckert, Fourier versus non-Fourier heat conduction in materials with a nonhomogeneous inner structure, J. Heat Transfer-Trans. ASME 122 (2) (2000) 363–365.
[9] W. Roetzel, N. Putra, S.K. Das, Experiment and analysis for non-Fourier conduction in materials with non-homogeneous inner structure, Int. J. Therm. Sci. 42 (6) (2003) 541–552.
[10] A.W. Richardson, C.G. Imig, B.L. Feucht, H.M. Hines, Relationship between deep tissue temperature and blood flow during electromagnetic irradiation, Arch. Phys. Med. Rehabil. 31 (1950) 19–25.
[11] R.B. Roemer, J.R. Oleson, T.C. Cetas, Oscillatory temperature response to constant power applied to canine muscle, Am. J. Physiol. 249 (2) (1985) R153–R158.
[12] K. Mitra, S. Kumar, A. Vedavarz, M.K. Moallemi, Experimental evidence of hyperbolic heat conduction in processed meat, J. Heat Transfer, Trans. ASME 117 (3) (1995) 568–573.
[13] E.V. Davydov, I.A. Lubashevsky, V.A. Milyaev, R.F. Musin, Nondiffusive heat transfer in muscle tissue 1 (1) (2001), preliminary results, arXiv:cond-mat/0102006.
[14] M. Tilahun, E.P. Scott, B. Vick, The question of thermal waves in heterogeneous and biological materials, Am. Soc. Mech. Eng., Bioeng. Div. (Publ.) BED 44 (1999) 145–152.
[15] P.J. Antaki, New interpretation of non-Fourier heat conduction in processed meat, J. Heat Transfer 127 (2) (2005) 189–193.
[16] J. Liu, X. Chen, L.X. Xu, New thermal wave aspects on burn evaluation of skin subjected to instantaneous heating, IEEE Trans. Biomed. Eng. 46 (4) (1999) 420–428.
[17] L.X. Xu, J. Liu, Discussion of non-equilibrium heat transfer in biological systems, in: Advances in Heat and Mass Transfer in Biotechnology, Proceedings of the 1998 ASME International Mechanical Engineering Congress and Exposition, Anaheim, CA, USA, 1998, pp. 13–17.
[18] H.S. Tharp, W. Zhang, Analytical study of temperature oscillations in living tissue, IEEE Trans. Biomed. Eng. 40 (1) (1993) 108–110.
[19] Z.S. Deng, J. Liu, Blood perfusion-based model for characterizing the temperature fluctuations in living tissue, Phys. A STAT Mech. Appl. 300 (3–4) (2001) 521–530.
[20] C. Chen, R.B. Roemer, A thermo-pharmacokinetic model of tissue temperature oscillations during localized heating, Int. J. Hyperther. 21 (2) (2005) 107–124.
[21] J. Liu, X.X. Zhang, C.C. Wang, W.Q. Lu, Engineering investigation on medical application approaches f or the thermal wave effects in living tissue, Space Med. Med. Eng. 10 (2) (1997) 135–139.
[22] J. Liu, Z.P. Ren, C.C. Wang, Simulating experimental study on the mechanisms of temperature oscillation in living tissue, J. Basic Sci. Eng. 4 (2) (1996) 173–182.
[23] J. Liu, C.C. Wang, Z.P. Ren, Theory and experiments on temperature oscillations effects in living tissue, J. Tsinghua Univ. (Sci & Tech) 2 (1997) 91–95.

[24] T.-C. Shih, H.-S. Kou, C.-T. Liauh, W.-L. Lin, The impact of thermal wave characteristics on thermal dose distribution during thermal therapy: A numerical study, Med. Phys. 32 (9) (2005) 3029–3036.
[25] A.R. Moritz, F.C. Henriques, Study of thermal injuries II. The relative importance of time and source temperature in the causation of cutaneous burns, Am. J. Pathol. 23 (1947) 695–720.
[26] H.H. Pennes, Analysis of tissue and arterial blood temperatures in the resting human forearm, J. Appl. Physiol. 1 (1948) 93–122.
[27] J. Herivel, Joseph Fourier: Face aux objections contre sa theorie de la chaleur: Bibliotheque Nationale, Paris, 1980.
[28] M.N. Ozisik, D.Y. Tzou, On the Wave Theory in Heat Conduction, Anaheim, CA, USA, 1992, pp. 13–27.
[29] T.Q. Qiu, C.L. Tien, Short-pulse laser heating on metals, Int. J. Heat Mass Transfer 35 (3) (1992) 719–726.
[30] A. Vedavarz, S. Kumar, M.K. Moallemi, Significance of non-Fourier heat waves in conduction, J. Heat Transfer, Trans. ASME 116 (1) (1994) 221–224.
[31] P.J. Antaki, Importance of nonFourier heat conduction in solid-phase reactions, Combust. Flame 112 (3) (1998) 329–341.
[32] J. Liu, W.Q. Lu, Dual reciprocity boundary element method for solving thermal wave model of bioheat transfer, Space Med. Med. Eng. 10 (6) (1997) 391–395.
[33] W.-Q. Lu, J. Liu, Y. Zeng, Simulation of the thermal wave propagation in biological tissues by the dual reciprocity boundary element method, Eng. Anal. Boundary Elem. 22 (3) (1998) 167–174.
[34] W.-Q. Lu, J. Liu, Y. Zeng, Extension of the dual reciprocity boundary element method to simulate thermal wave propagation in biological tissu, J. Eng. Thermophys. 19 (6) (1998) 728–731.
[35] P.M. Morse, H. Feshbach, Methods of Theoretical Physics, vol. 1, McGraw-Hill, New York, 1953.
[36] C. Cattaneo, A form of heat conduction equation which eliminates the paradox of instantaneous propagation, Comp. Rend. 247 (1958) 431–433.
[37] P. Vernotte, Les paradoxes de la theorie continue de l'equation de la chaleur, Comp. Rend. 246 (1958) 3154–3155.
[38] M. Chester, Second sound in solid, Phvs. Rev. 131 (1963) 2013–2015.
[39] H.D. Weymann, Finite speed of propagation in heat conduction, diffusion and viscous shear motion, Am. J. Phys. 35 (1967) 488–496.
[40] D.Y. Tzou, Macro- to Micro-scale Heat Transfer: The Lagging Behavior, Taylor and Francis, Washington, DC, 1997.
[41] D. Yu Tzou, An engineering assessment to the relaxation time in thermal wave propagation, Int. J. Heat Mass Transfer 36 (7) (1993) 1845–1851.
[42] M.N. Ozisik, D.Y. Tzou, On the wave theory in heat conduction, ASME J. Heat Transfer 116 (1994) 526–535.
[43] D.Y. Tzou, An engineering assessment to the relaxation time in thermal wave propagation, Int. J. Heat Mass Transfer 36 (7) (1993) 1845–1851.
[44] D.Y. Tzou, Thermal shock phenomena under high-rate response in solids, in: C.L. Tien (Ed.), Annual Review of Heat Transfer, Hemisphere, Washington, DC, 1992, pp. 111–185.
[45] S. Sieniutycz, The variational principles of classical type for non-coupled non-stationary irreversible transport processes with convective motion and relaxation, Int. J. Heat Mass Transfer 20 (11) (1977) 1221–1231.
[46] Y. Taitel, On the parabolic, hyperbolic and discrete formulation of the heat conduction equation, Int. J. Heat Mass Transfer 15 (2) (1972) 369–371.
[47] N.V. Antonishyn, M.A. Geller, A.L. Parnas, Hyperbolic heat conduction equation for disperse system, Inzhenerno Fiz. Zh. 26 (3) (1974) 503–508.
[48] B.M. Raspopov, Control of some transfer processes, Inzhenerno Fiz. Zh. 12 (1967) 444.
[49] A.M. Brazhnikov, V.A. Karpychev, A.V. Luikova, One engineering method of calculating heat conduction processes, Inzhenerno Fiz. Zh. 28 (4) (1975) 677–680.
[50] S. Michalowski, E. Mitura, W. Kaminski, The application of mathematical method to describe the kinetics of drying, Hungarian J. Indus. Chem. 10 (1982) 387.
[51] E. Mitura, S. Michalowski, W. Karnlnski, A mathematical model of convection drying in Falling drying rate period, Dry. Technol. 6 (1988) 113–137.
[52] A.V. Luikov, Application of irreversible thermodynamics methods to investigation of heat and mass transfer, Int. J. Heat Mass Transfer 9 (2) (1966) 139–152.
[53] A.J. Stratigos, J.S. Dover, Overview of Lasers and Their Properties vol. 13 (2000) 2–16.
[54] D.W. Tang, N. Araki, The wave characteristics of thermal conduction in metallic films irradiated by ultra-short laser pulses, J. Phys. D: Appl. Phys. 29 (1996) 2527.
[55] J. Liu, X.X. Zhang, W.Q. Lu, C.C. Wang, The thermal pulse decay method for invasive measurement of blood perfusion of tissue in vivo, Progr. Nat. Sci. 9 (2) (1999) 179–184.
[56] T.C. Zhu, X.Z. Feng, Numerical analysis of the relationship between blood flow coefficient and living tissue thermal behavior, Chin. J. Hemorheol. 11 (3) (2001) 182–183.
[57] Z.S. Deng, J. Liu, Non-Fourier heat conduction effect on prediction of temperature transients and thermal stress in skin cryopreservation, J. Therm. Stress. 26 (8) (2003) 779–798.
[58] J.C. Chato, R.C. Lee, The future of biothermal engineering, Ann. N.Y. Acad. Sci. 858 (1998) 1–17.
[59] J. Liu, Preliminary survey on the mechanisms of the wave-like behaviors of heat transfer in living tissues, Forsch. Ingenieurwesen/ Eng. Res. 66 (1) (2000) 1–10.
[60] N. Ma, S. Jiang, H. Li, X. Zhang, Analysis of non-flourier effect and laser-induced thermal damage of laser-irradiated layered human skin tissue, Space Med. Med. Eng. 16 (2) (2003) 133–137.
[61] Y. Bayazitoglu, G.P. Peterson, Fundamental issues in hyperbolic heat conduction, ASME HTD, 1992, p. 227.
[62] D.Y. Tzou, M.N. Ozisik, R.J. Chiffelle, The lattice temperature in the microscopic two-step model, J. Heat Transfer 116 (1994) 1034–1038.
[63] C. Koerner, H.W. Bergmann, Physical defects of the hyperbolic heat conduction equation, Appl. Phys. A: Mater. Sci. Process. 67 (4) (1998) 397–401.
[64] S. Godoy, L.S. García-Colín, Nonvalidity of the telegrapher's diffusion equation in two and three dimensionsfor crystalline solids, Phys. Rev. E 55 (1997) 2127–2131.
[65] D.Y. Tzou, A unified field approach for heat conduction from macro- to micro-scales, J. Heat Transfer, Trans. ASME 117 (1) (1995) 8–16.
[66] D.Y. Tzou, Experimental support for the lagging behavior in heat propagation, J. Thermophys. Heat Transfer 9 (1995) 686–693.
[67] R. Quintanilla, R. Racke, A note on stability in dual-phase-lag heat conduction, Int. J. Heat Mass Transfer 49 (7–8) (2006) 1209–1213.
[68] D.Y. Tzou, K.S. Chiu, Temperature-dependent thermal lagging in ultrafast laser heating, Int. J. Heat Mass Transfer 44 (9) (2001) 1725–1734.
[69] F.C. Henriques, A.R. Moritz, Studies of thermal injury, 1. The conduction of heat to and through skin and the temperatures attained therein. A theoretical and an experimental investigation, Am. J. Pathol. 23 (1947) 531–549.
[70] F.C. Henriques, Study of thermal injuries V., The predictability and the significance of thermally induced rate processes leading to irreversible epidermal injury, Arch. Pathol. 43 (1947) 489–502.
[71] N.T. Wright, On a relationship between the Arrhenius parameters from thermal damage studies, J. Biomech. Eng. 125 (2003) 300–304.
[72] K.R. Diller, J.A. Pearce, Issues in modeling thermal alterations in tissues, Ann. N.Y. Acad. Sci. 888 (1999) 153–164.
[73] F. Despa, D.P. Orgill, J. Neuwalder, R.C. Lee, The relative thermal stability of tissue macromolecules and cellular structure in burn injury, Burns 31 (2005) 568–577.
[74] F. Xu, Thermomechanical analysis of skin tissue, PhD First Year Report, Cambridge, UK Engineering Department, Cambridge University, 2005.
[75] F. Xu, T. Wen, K.A. Seffen, T.J. Lu, Biothermomechanics of skin tissue, J. Mech. Phys. Solids (2007).

[76] J.D. Rigal, J. Leveque, In vivo measurement of the stratum corneum elasticity, Bioeng. Skin 1 (1985) 13–23.
[77] N. Magnenat-Thalmann, P. Kalra, J.L. Leveque, R. Bazin, D. Batisse, B. Querleux, A computational skin model: fold and wrinkle formation, IEEE Trans. Inf. Technol. Biomed. 6 (4) (2002) 317–323.
[78] A. Patapoutian, A.M. Peier, G.M. Story, V. Viswanath, Thermo TRP channels and beyond: mechanisms of temperature sensation, Nat. Rev. Neurosci. 4 (8) (2003) 529–539.
[79] L. Kruger, E.R. Perl, M.J. Sedivec, Fine structure of myelinated mechanical nociceptor endings in cat hairy skin, J. Comp. Neurol. 198 (1) (1981) 137–154.
[80] N.C. James, A.M. Richard, Neurobiology of Nociceptors, Oxford University Press, Oxford, 1996.
[81] H.J. Van, J. Gybels, C nociceptor activity in human nerve during painful and non painful skin stimulation, J. Neurol. Neurosurg. Psychiatr. 44 (7) (1981) 600–607.
[82] A.V.S. Reuck, J. Knight, Touch, Heat and Pain, Churchill Ltd., 1966.
[83] K.-C. Liu, Analysis of dual-phase-lag thermal behaviour in layered films with temperature-dependent interface thermal resistance, J. Phys. D: Appl. Phys. 38 (19) (2005) 3722–3732.
[84] F.A. Duck, Physical Properties of Tissue: A Comprehensive Reference Book, Academic Press, 1990.
[85] D.A. Torvi, J.D. Dale, A finite element model of skin subjected to a flash fire, J. Biomech. Eng. 116 (3) (1994) 250–255.
[86] A. Delalleau, G. Josse, J.M. Lagarde, H. Zahouani, J.M. Bergheau, Characterization of the mechanical properties of skin by inverse analysis combined with the indentation test, J. Biomech. 39 (9) (2006) 1603–1610.
[87] F.M. Hendriks, D. Brokken, C.W. Oomens, D.L. Bader, F.P. Baaijens, The relative contributions of different skin layers to the mechanical behavior of human skin in vivo using suction experiments, Med. Eng. Phys. 28 (3) (2006) 259–266.
[88] W. Elkins, J.G. Thomson, Instrumented Thermal Manikin, Acurex Corporation, Aerotherm Division Report AD-781, 1973, p. 176.
[89] W. Roetzel, Y. Xuan, Transient response of the human limb to an external stimulus, Int. J. Heat Mass Transfer 41 (1) (1998) 229–239.
[90] P. Sejrsen, Measurement of cutaneous blood flow by freely diffusible radioactive isotopes, Dan. Med. Bull. 18 (1972) 1–38.
[91] S. Dahan, J.M. Lagarde, V. Turlier, L. Courrech, S. Mordon, Treatment of neck lines and forehead rhytids with a nonablative 1540-nm Er:glass laser: A controlled clinical study combined with the measurement of the thickness and the mechanical properties of the skin, Dermatol. Surg. 30 (6) (2004) 872–879.
[92] J.T. Whitton, J.D. Everall, The thickness of the epidermis, Brit. J. Dermatol. 89 (1973) 467–476.
[93] C.E. Fugitt, A rate process of thermal injury, Armed Forces Special Weapons Project AFSWP-606, 1955.
[94] A.M. Stoll, L.C. Greene, Relationship between pain and tissue damage due to thermal radiation, J. Appl. Phys. 14 (3) (1959) 373–382.
[95] J.A. Weaver, A.M. Stoll, Mathematical model of skin exposed to thermal radiation, Aerosp. Med. 40 (1) (1969) 24–30.
[96] A.K. Mehta, F.C. Wong, Measurement of Flammability and Burn Potential of Fabrics, Massachusetts Institute of Technology, Cambridge, Massachusetts, 1973.
[97] A.N. Takata, J. Rouse, T. Stanley, Thermal Analysis Program, I.I.T., Chicago, 1973.
[98] Y.C. Wu, A Modified Criterion for Predicting Thermal Injury, National Bureau of Standards, Washington, 1982.
[99] J.A. Pearce, W.-F. Cheong, K. Pandit, T.J. McMurray, S.L. Thomsen, Kinetic models for coagulation processes: determination of rate coefficients in vivo, in: Lasers in Dermatology and Tissue Welding, Los Angeles, CA, USA, 1991, pp. 27–33.
[100] J.A. Pearce, S. Thomsen, H. Vijverberg, T. Magnusen, Quantitative Measurement of Thermal Damage: Birefringence Changes in Thermally Coagulated Collagen, New Orleans, LA, USA, 1993, pp. 141–144.